Article

Cell Reports

Microbiota Depletion Impairs Thermogenesis of Brown Adipose Tissue and Browning of White Adipose Tissue

Graphical Abstract

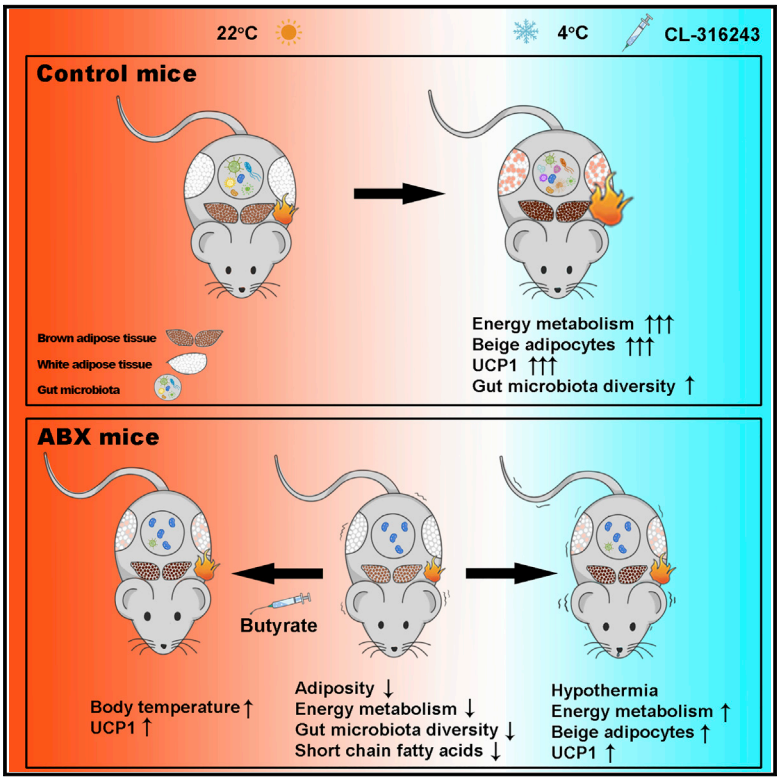

Highlights

- Mice lacking gut microbiota have impaired UCP1-dependent thermogenesis in cold
- These effects are replicated in germ-free mice treated with CL-316243
- IL-4 has no differential effect on energy metabolism in either control or ABX mice
- Gavage of ABX mice with butyrate partially rescues the effects on BAT recruitment

Authors

Baoguo Li, Li Li, Min Li, ..., Wanzhu Jin, Guanghou Shui, John R. Speakman

Correspondence

j.speakman@genetics.ac.cn

In Brief

Li et al. use different antibiotic recipes and germ-free mice to demonstrate the dependence of UCP1-dependent thermogenesis in the cold on the presence of a healthy gut microbiome. Gavage with butyrate partly rescues the effect, indicating a role for this molecule in normal thermogenic responses to low temperature.

Li et al., 2019, Cell Reports *26*, 2720–2737
March 5, 2019
https://doi.org/10.1016/j.celrep.2019.02.015

CellPress

OPEN ACCESS
CellPress

Cell Reports
Article

Microbiota Depletion Impairs Thermogenesis of Brown Adipose Tissue and Browning of White Adipose Tissue

Baoguo Li,[1,2,6] Li Li,[1,2,6] Min Li,[1,2,3,6] Sin Man Lam,[1,6] Guanlin Wang,[1,2,3] Yingga Wu,[1,2,3] Hanlin Zhang,[2,4] Chaoqun Niu,[1] Xueying Zhang,[1,2,3] Xue Liu,[1,2] Catherine Hambly,[3] Wanzhu Jin,[4] Guanghou Shui,[1] and John R. Speakman[1,3,5,7,*]

[1]State Key Laboratory of Molecular Developmental Biology, Institute of Genetics and Developmental Biology, Chinese Academy of Sciences, Beijing 100101, PRC
[2]University of Chinese Academy of Sciences, Beijing 100049, PRC
[3]Institute of Biological and Environmental Sciences, University of Aberdeen, Aberdeen AB24 2TZ, UK
[4]Key Laboratory of Animal Ecology and Conservation Biology, Institute of Zoology, Chinese Academy of Sciences, Beijing 100101, PRC
[5]CAS Center for Excellence in Animal Evolution and Genetics (CCEAEG), Beijing 100101, PRC
[6]These authors contributed equally
[7]Lead Contact
*Correspondence: j.speakman@genetics.ac.cn
https://doi.org/10.1016/j.celrep.2019.02.015

SUMMARY

The relation between gut microbiota and the host has been suggested to benefit metabolic homeostasis. Brown adipose tissue (BAT) and beige adipocytes facilitate thermogenesis to maintain host core body temperature during cold exposure. However, the potential impact of gut microbiota on the thermogenic process is confused. Here, we evaluated how BAT and white adipose tissue (WAT) responded to temperature challenges in mice lacking gut microbiota. We found that microbiota depletion via treatment with different cocktails of antibiotics (ABX) or in germ-free (GF) mice impaired the thermogenic capacity of BAT by blunting the increase in the expression of uncoupling protein 1 (UCP1) and reducing the browning process of WAT. Gavage of the bacterial metabolite butyrate increased the thermogenic capacity of ABX-treated mice, reversing the deficit. Our results indicate that gut microbiota contributes to upregulated thermogenesis in the cold environment and that this may be partially mediated via butyrate.

INTRODUCTION

In the last decade, it has been shown that adult humans have active depots of brown adipose tissue (BAT) and that the size and activity of such depots is reduced in people with obesity (Cypess et al., 2009; Guilherme et al., 2008; Nedergaard et al., 2007; Pfannenberg et al., 2010; Saito et al., 2009). This has refueled speculation that obesity may be caused by lowered BAT activity (Speakman, 2013), as was originally speculated in the 1970s (Rothwell and Stock, 1979). A diverse microbial community resides in the alimentary tracts of all mammalian species, comprising mainly bacteria but also including fungi, viruses, archaea, and protozoa. Normally, gut microbiota refers to anaerobic bacteria, which are numerically dominant (Maier et al., 2014; Qin et al., 2010). The host gut provides a suitable habitat for particular bacterial groups, and in turn, gut microbiota contributes nutrients and energy to the host (den Besten et al., 2013; Donohoe et al., 2011; Flint et al., 2012; Seedorf et al., 2014). Recent reports indicated that the composition of gut microbiota alters during cold challenge, and the transfer of "cold microbiota" increases white adipose tissue (WAT) browning, energy expenditure, and cold tolerance (Chevalier et al., 2015). The same group also reported that both antibiotic-treated and germ-free mice have a browning phenotype in their WAT at room temperature (22°C) and at thermoneutrality (30°C), suggesting that depleting microbiota enhances thermogenic capacity. They concluded that the elimination of microbiota increased eosinophil infiltration and enhanced type 2 cytokine signaling and M2 macrophage polarization in WAT, which drives the browning process (Suárez-Zamorano et al., 2015). Most previous studies have focused on the browning of WAT, but the impact of microbiota on the interscapular BAT has been less studied. This is a serious omission because BAT is the major source of adaptive thermogenic heat production (Cannon and Nedergaard, 2004). This raises the obvious question of whether BAT thermogenesis is responsive to microbiota composition and what impact the microbiota has on both BAT and WAT under different temperature challenges (Wang et al., 2016). This question is made all the more important because recent work has questioned whether macrophages synthesize catecholamines and concluded that they do not affect adaptive thermogenesis (Fischer et al., 2017). However, this was the primary mechanism previously suggested to link microbiota to adaptive browning. Accordingly, the aim of the present study was to re-evaluate the effects of gut microbiota on the adaptive thermogenesis of mice and to further evaluate the role of type 2 cytokine signaling in the regulation of brown and beige adipocyte activity. We show that microbiota depletion does not promote the browning of WAT at room temperature; conversely, the adaptive thermogenic capacity of BAT and WAT under cold challenge is impaired when the microbiota is depleted.

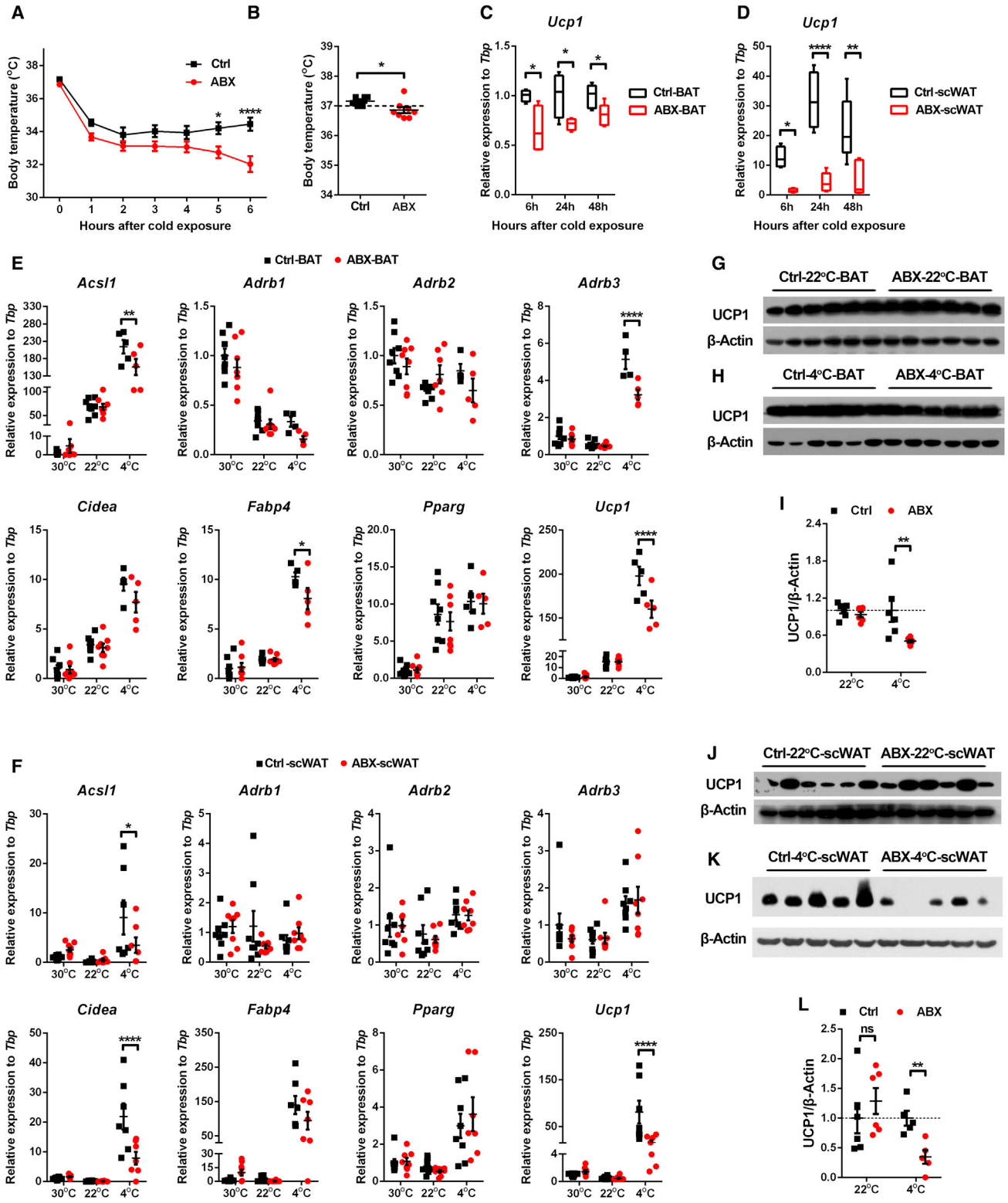

Figure 1. Gut Microbiota Depletion Impairs Thermoregulation

(A and B) The changes in rectal temperature during 4°C cold stimulation (A) and in room temperature (B) between control and ABX mice (n = 6 in the control group and n = 8 in the ABX group).

(C and D) The changes of *Ucp1* gene expression in the BAT (C) and scWAT (D) from control and ABX groups under cold stimulation (n = 4 per group).

(legend continued on next page)

RESULTS

Gut Microbiota Depletion Damages Thermoregulation

To explore the effect of gut microbiota depletion on thermogenesis in mice, we administered an antibiotic cocktail (ABX) in the drinking water (Abt et al., 2012; Hill et al., 2012; Suárez-Zamorano et al., 2015) for 3–4 weeks. Immediately following antibiotic treatment, body weight dropped and then 1 week later slowly recovered (Figures S1A and S1B). Microbiota depletion significantly changed the morphology of the small intestine, cecum, and colon (Figure S1C). These components of the intestines of ABX mice were significantly longer (2-way ANOVA, $F_{1,21}$ = 55.43, $p < 0.0001$) and the cecum was highly enlarged (2-way ANOVA, $F_{1,21}$ = 55.43, $p < 0.05$) (Figure S1D). The morphology of the fecal pellets was also significantly changed (Figure S1E). To determine the impacts on thermogenic function, we conducted a cold-response experiment. Compared to the specific-pathogen-free mice housed under conventional conditions (control), ABX mice had impaired thermoregulation when acutely exposed to an ambient temperature of 4°C (Figure 1A). Control mice were able to sustain body temperature at a significantly higher level than the ABX-treated individuals (2-way ANOVA, $F_{12,72}$ = 8.863, $p < 0.0001$). At room temperature, ABX mice also had significantly lower core body temperatures (2-tailed Mann-Whitney test, p = 0.027) (Figure 1B). This was consistent with the *Ucp1* gene expression, which was significantly lower in both BAT (2-way ANOVA, $F_{1,22}$ = 54.98, $p < 0.0001$) and subcutaneous WAT (scWAT) (2-way ANOVA, $F_{1,22}$ = 8.938, p = 0.0068) of ABX mice under cold stimulation for 48 h (Figures 1C and 1D). In contrast to a previous study (Suárez-Zamorano et al., 2015), we failed to observe any effect of ABX treatment on *Ucp1* gene expression in both BAT (2-way ANOVA, $F_{1,37}$ = 13.18, $p > 0.9999$) and scWAT (2-way ANOVA, $F_{1,42}$ = 8.817, $p > 0.9999$) at room temperature (22°C) and thermoneutrality (30°C) (Figures 1E and 1F). Protein levels of uncoupling protein 1 (UCP1) were also not significantly elevated in scWAT (2-way ANOVA, $F_{1,18}$ = 0.8266, p = 0.603) of ABX mice compared to control mice at 22°C (Figures 1G and 1J). Moreover, the protein levels of UCP1 were significant lower in ABX mice after cold stimulation in both BAT (2-way ANOVA, $F_{1,20}$ = 8.212, p = 0.0037) and scWAT (2-way ANOVA, $F_{1,18}$ = 0.8266, p = 0.0079) (Figures 1H and 1K), which is consistent with their impaired ability to maintain body temperature under cold challenge (Figure 1A). These data indicate that the depletion of microbiota impairs the adaptive thermogenic capacity of both BAT and scWAT. We also did not observe any differences in expression of a core set of thermogenic genes in perigonadal visceral adipose tissue (pgVAT) at 22°C and 4°C between the control and ABX groups (Figure S1F). However, expression of some genes in pgVAT was higher in ABX at 30°C (Figure S1F). Consistent with previous reports, the expression levels of *Ucp1* in different tissues indicated that BAT is the key tissue for thermogenesis compared to scWAT and pgVAT (Cannon and Nedergaard, 2004) (Figure S1G).

Methionine sulfoxide, fructose 2,6-bisphosphate (Sobrino et al., 1988), cyclic guanosine monophosphate (cGMP) (Hoffmann et al., 2015), and pantothenic acid (vitamin B5) levels in serum were significantly higher in control mice at both 22°C and 4°C compared to ABX individuals. In contrast, 11β-prostaglandin F2αwas significantly lower in control mice at both 22°C and 4°C. A previous study reported that the gut microbiota may regulate tryptophan metabolism through tryptophan hydroxylase and promote serotonin biosynthesis (Yano et al., 2015). Both germ-free (GF) and ABX mice displayed deficient peripheral serotonin and higher tryptophan concentrations. Consistent with previous studies, we also found that tryptophan was significantly elevated in ABX-treated mice (Figure S1H; Table S1). Our results suggest that microbiota depletion represses the expression of *Ucp1*, and UCP1 thus impairs adaptive thermogenesis in BAT and scWAT at both 22°C and 4°C.

Gut Microbiota Depletion Reduces the Energy Metabolism of the Host

Many studies previously reported that gut microbiota may influence diverse biological phenomena (Flint et al., 2012; Sommer and Bäckhed, 2013; Tremaroli and Bäckhed, 2012; Zhao, 2013). To evaluate whether ABX-mediated impairment of thermogenesis of BAT and scWAT contributes to whole-body energy expenditure, we used indirect calorimetry. At 22°C, ABX mice had ~13% lower oxygen consumption (VO_2) (Figures 2A and 2C) compared to control mice (2-way ANOVA, $F_{2,35}$ = 23.34, p = 0.0304) without any significant differences in the respiratory exchange ratio (RER) (2-way ANOVA, $F_{2,31}$ = 0.1243, p = 0.5681) (Figures 2D and 2F) or physical activity (2-way ANOVA, $F_{2,29}$ = 1.333, $p > 0.9999$) (Figures 2G and 2I). Compared to 22°C, cold exposure (4°C) enhanced energy expenditure in both control and ABX mice, which likely reflects the activation of cold-induced thermogenesis. However, ABX mice had ~17% lower oxygen consumption (Figures 2B and 2C) compared to control mice at 4°C (2-way ANOVA, $F_{2,35}$ = 23.34, $p < 0.0001$), again, with no impact on the RER (Figures 2E and 2F) (2-way ANOVA, $F_{2,31}$ = 0.1243, p = 0.8186) and physical activity (2-way ANOVA, $F_{2,29}$ = 1.333, p = 0.7487) (Figures 2H and 2I). At the same time, ABX mice had smaller metabolic changes in response to the circadian cycle compared to control mice at 4°C (Figure 2B). To evaluate whether the lower body mass following the initial antibiotic treatment influenced the thermogenesis process (Figures S1A and S1B), we generated a new mice group that was pair fed (PF) to match the energy absorption of the ABX group each day. The similar pattern of change in body weight between ABX and PF mice (Figure S2A) indicated that this pair feeding was effective. Both ABX and PF groups had lower body weight compared to control individuals (2-way

(E and F) The thermogenic gene expression in the BAT (E) and scWAT (F) from control and ABX groups under different ambient temperatures (n = 5–10 per group). (G–L) Representative western blot and quantification of UCP1 in the BAT (22° in G, 4° in H and I) and scWAT (22°C in J, 4°C in K and L) from control and ABX groups under different ambient temperatures (n = 5–6 per group).

The results shown are representative of 2 independent experiments (A–D) or 3 independent experiments (E–L). All results are given as mean ± SEM and statistical analyses were performed using the Student's t test and regular one-way or two-way ANOVA. Differences with $p < 0.05$ were considered to be significant. *$p < 0.05$, **$p < 0.01$, ***$p < 0.001$, and ****$p < 0.0001$. See also Figure S1 and Table S1.

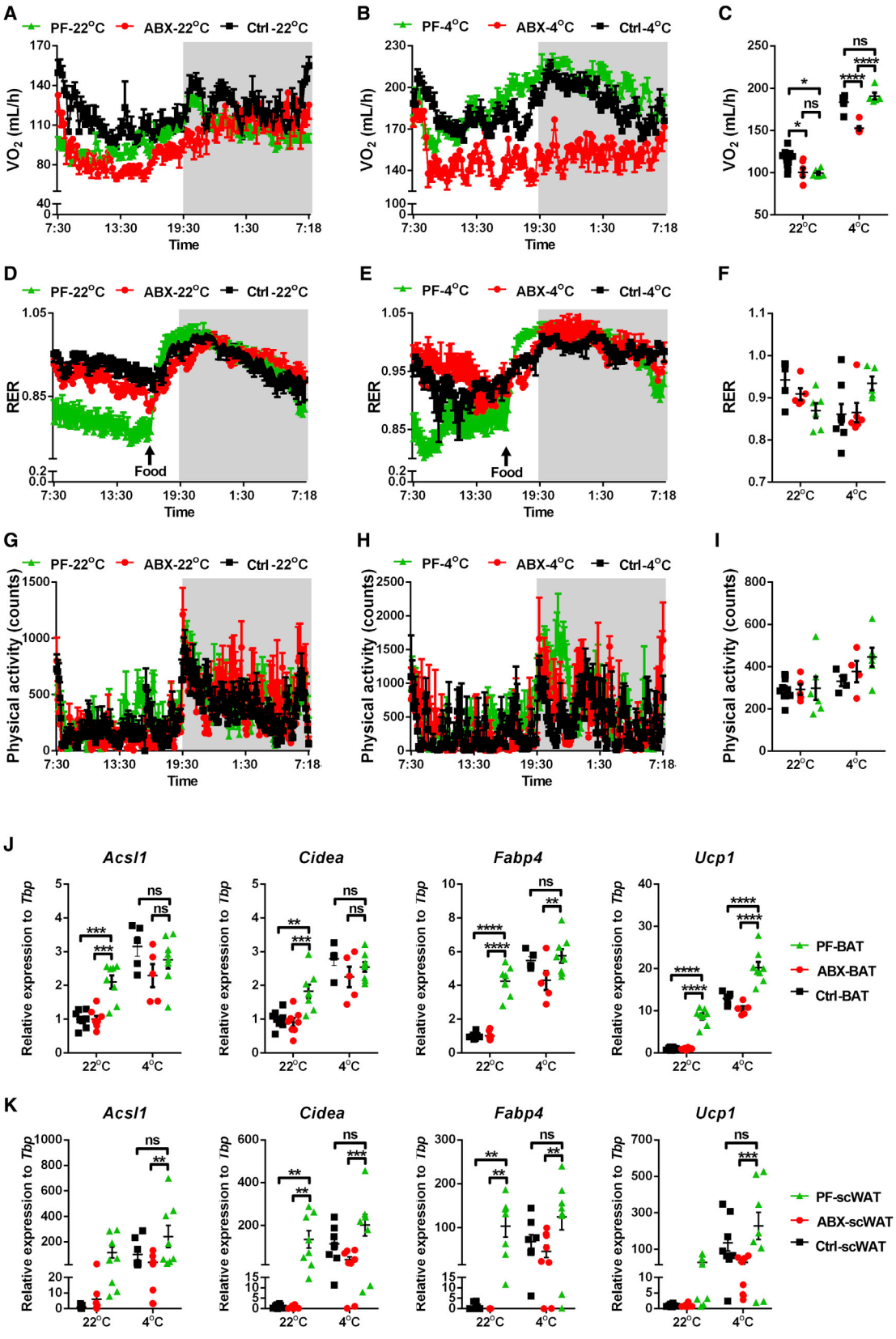

(legend on next page)

repeated-measures ANOVA, $F_{59,1,593} = 125.9$, $p < 0.0001$) (Figure S2A) and fat mass from different anatomic sites (Figures S2E–S2G). Based on the difference in daily energy intake (Figure S2B) and the fecal energy losses (Figure S2C), ABX mice had a significantly lower assimilation efficiency (2-way ANOVA, $F_{17,442} = 8.617$, $p < 0.0001$) (Figure S2D).

At 22°C, there was no significant difference in the oxygen consumption rate between PF and ABX mice (2-way ANOVA, $F_{2,35} = 23.34$, $p > 0.9999$) (Figures 2A and 2C). However, PF mice had a significantly higher cold-induced energy expenditure (~25% higher) compared to ABX mice (2-way ANOVA, $F_{2,35} = 23.34$, $p < 0.0001$) (Figure 2C). During the daytime, the RER of the PF group was lower (1-way ANOVA, $F_{5,295} = 126$, $p < 0.0001$) than the control and ABX groups, partly because they ate their ration of food in the night and hence had no food available in the day. The physical activity of PF mice also showed increasing food anticipation behavior at ~16:30 h (1-way ANOVA, $F_{5,50} = 11.53$, $p < 0.0001$), which was 30 min before the feed time of 17:00 h (Figures 2G and 2H), but total physical activity was not significantly different (2-way ANOVA, $F_{2,29} = 1.333$, $p = 0.2794$) (Figure 2I).

Furthermore, we compared expression of the core thermogenic genes in BAT and scWAT and found that PF mice had a significantly higher expression of *Ucp1* compared to ABX mice (Figures 2J, 2K, and S2H). These data for PF mice suggested that energy intake and the temporarily lowered body weight observed in ABX mice were not the cause of lower energy expenditure and thermogenic capacity. Instead, the data on whole-body energy expenditure (Figures 2A–2C) and UCP1 protein expression in BAT and scWAT (Figures 1G–1L) supported the idea that the depletion of microbiota impaired the thermogenesis of BAT and scWAT.

Alternatively Activated Macrophages Do Not Affect Energy Metabolism and Thermogenesis in ABX Mice

According to previous studies, type 2 cytokine signaling and alternative macrophage activation (M2) play a key role in the browning process of scWAT across the temperature range from 30°C to 4°C, and these may mediate the impact of microbiota on thermoregulation (Nguyen et al., 2011; Suárez-Zamorano et al., 2015). We therefore measured the gene expression of M1 and M2 markers (*CD274*, *Nos2*, *Arg1*, *Mrc1*, *Clec10*, and *Ccr3*), a marker of eosinophils (*SiglecF*), and the profiles of some type 2 cytokines (interleukin-4 [*IL-4*], *IL-5*, and *IL-33*) using qPCR. We observed no significant differences of these genes in BAT, scWAT, and pgVAT between control and ABX mice at different environment temperatures (Figures 3A, 3B, and S3A). By using flow cytometry (Figures S3B and S3C), we also found no evidence for the enhancement of eosinophil and alternative activated macrophage populations in BAT, scWAT, and pgVAT of the control mice after cold stimulation (Figures 3C–3E). Conversely, we noticed that the portion of M2 macrophages in total immune cells was significantly decreased in BAT (2-way ANOVA, $F_{1,20} = 0.5253$, $p = 0.0008$) and scWAT (2-way ANOVA, $F_{1,20} = 0.1078$, $p < 0.0001$) in control mice at 4°C compared to that at 22°C. However, ABX mice had an increase of alternative activated macrophages in BAT (2-way ANOVA, $F_{1,20} = 0.5253$, $p < 0.0001$), scWAT (2-way ANOVA, $F_{1,20} = 0.1078$, $p = 0.0006$), and pgVAT (2-way ANOVA, $F_{1,20} = 0.6391$, $p = 0.0168$) (Figures 3C–3E) at 4°C compared to 22°C. At 22°C, ABX mice had fewer M2 macrophages in BAT (2-way ANOVA, $F_{1,20} = 0.5253$, $p < 0.0001$), scWAT (2-way ANOVA, $F_{1,20} = 0.1078$, $p < 0.0001$), and pgVAT (2-way ANOVA, $F_{1,20} = 36.86$, $p < 0.0001$) compared to control mice (Figures 3C and 3D). Consistent with a previous study (Suárez-Zamorano et al., 2015), we found that ABX mice had significantly more eosinophils in scWAT (2-way ANOVA, $F_{1,20} = 0.8922$, $p = 0.0085$) and pgVAT (2-way ANOVA, $F_{1,20} = 16.77$, $p = 0.0012$) compared to control mice at 22°C (Figures 3D and 3E). After cold exposure, however, the population of eosinophils in ABX mice decreased and was significantly lower in BAT compared to control mice (2-way ANOVA, $F_{1,20} = 3.385$, $p = 0.0077$) (Figures 3D and 3E). We further measured several type 2 cytokines, including IL-4 (2-way ANOVA, $F_{1,43} = 0.3194$, $p = 0.5749$), IL-5 (2-way ANOVA, $F_{1,43} = 2.809$, $p = 0.1010$), and IL-33 (2-way ANOVA, $F_{1,43} = 2.125$, $p = 0.1524$) in scWAT by ELISA, but again, detected no significant difference between the control and the ABX groups (Figure 3F). To further assess the function of IL-4 on energy metabolism, we evaluated the metabolic effect of chronic IL-4 treatment in control and ABX mice housed at 23°C ± 1°C. We administered IL-4 (50 μg/kg) daily for 5 days. Measurement of the daily energy expenditure (DEE) during this period revealed no differential effect caused by IL-4 compared to PBS either in the control (2-way ANOVA, $F_{3,9} = 2.960$, $p = 0.7155$) group or in the ABX (2-way ANOVA, $F_{3,9} = 2.960$, $p = 0.9713$) group (Figure 3H); there was also no influence on RER and physical activity (Figures S3D and S3E). At the same time, IL-4 could induce M2 polarization in BAT and scWAT in the control group, confirming that IL-4 works well but did not increase the expression of *Ucp1* either in BAT or in scWAT from both groups (2-way ANOVA, $F_{3,30} = 70.75$, $p > 0.9999$) (Figures S3F–S3H). These results suggest that type 2 immune signaling and alternative macrophage activation are unlikely to make a direct contribution to adaptive thermogenesis, which is consistent with another recent study (Fischer et al., 2017).

To probe whether microbiota depletion induced lower-body fat mass (Figures S2E–S2G), leading to the impaired release of free fatty acids (the principal substrate for BAT thermogenesis), we measured circulating free fatty acid (FFA) and triglyceride

Figure 2. Gut Microbiota Depletion Reduces the Energy Metabolism of the Host

(A–I) Energy expenditure as determined by longitudinal and average oxygen consumption rate (22°C in A, 4°C in B and C), RER (22°C in D, 4°C in E and F), and total physical activity (22°C in G, 4°C in H and I) at different ambient temperatures (n = 8–10 in the control group, n = 6–8 in the ABX group, and n = 5–6 in the PF group).

(J and K) Gene expression analysis of thermogenic markers in BAT (J) and scWAT (K) (n = 5–8).

All of the results shown are representative of 2 independent experiments. All results are given as mean ± SEM and statistical analyses were performed using the Student's t test and regular one-way or two-way ANOVA. Differences with $p < 0.05$ were considered to be significant. *$p < 0.05$, **$p < 0.01$, ***$p < 0.001$, and ****$p < 0.0001$. See also Figure S2.

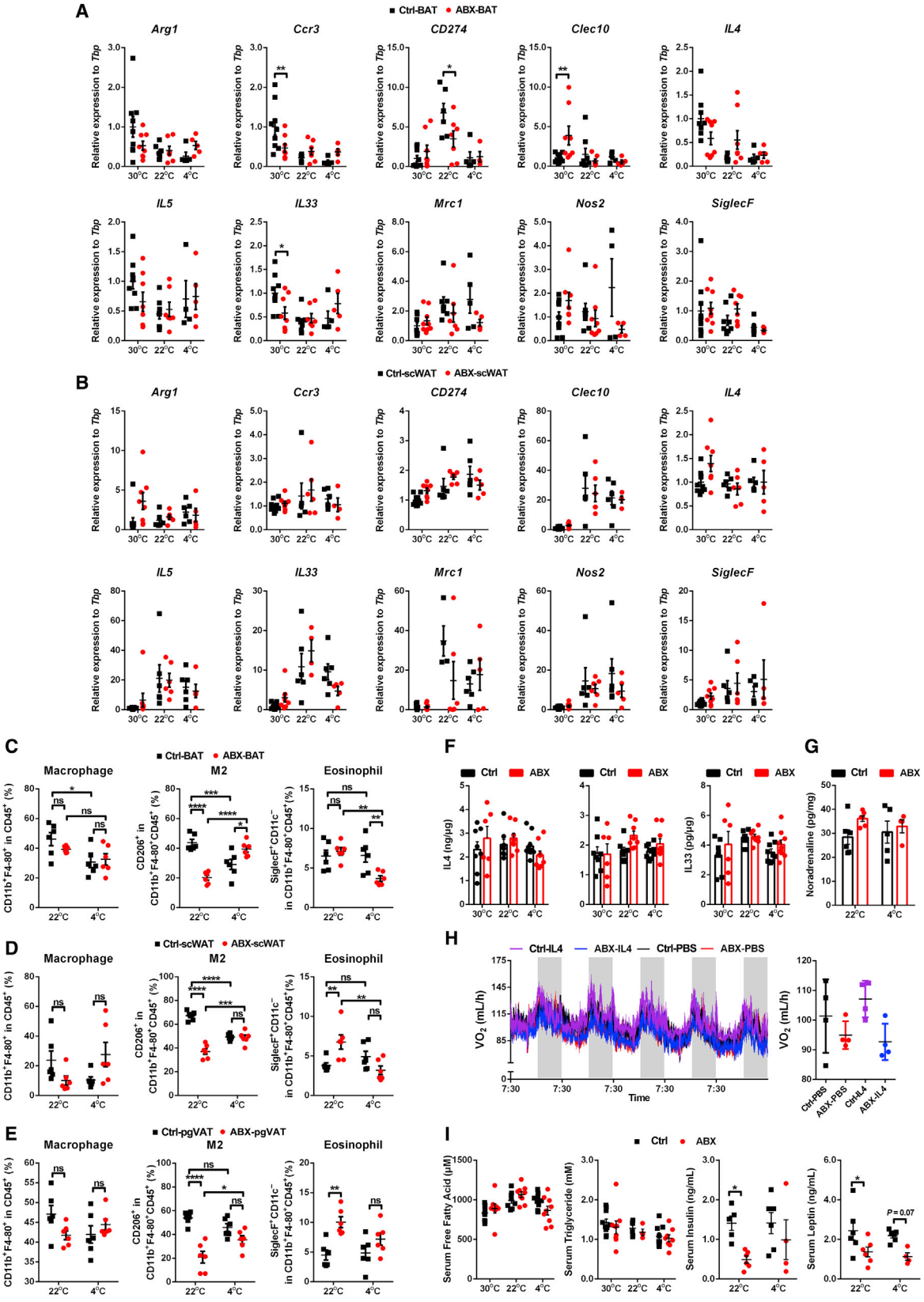

(legend on next page)

(TG) levels. No significant decrease in circulating FFA (2-way ANOVA, $F_{1,43}$ = 0.03571, p = 0.8518) and triglyceride (2-way ANOVA, $F_{1,40}$ = 0.8681, p = 0.3571) was observed when microbiota was depleted (Figure 3I). At the same time, insulin (2-way ANOVA, $F_{1,17}$ = 6.463, p = 0.0210) and leptin (2-way ANOVA, $F_{1,18}$ = 11.58, p = 0.0032) of ABX mice were significantly lower than control mice (Figure 3I). It was potentially the case, therefore, that microbiota depletion could have impeded the synthesis of noradrenaline, which is important for lipolysis and thermogenesis. We measured the noradrenaline content in scWAT, and there was no significant difference between control and ABX mice (2-way ANOVA, $F_{1,17}$ = 2.674, p = 0.1204) (Figure 3G). In summary, we failed to demonstrate any significant relation between thermogenesis and type 2 cytokine signaling and alternative macrophage activation. Moreover, microbiota depletion did not promote browning via the enhancement of type 2 cytokine signaling in scWAT. Even though at 22°C ABX mice had more eosinophils in scWAT and pgVAT than in control mice, we observed no difference in *Ucp1* expression. Our data are consistent with the recent report that type 2 cytokines have no function in thermogenesis (Fischer et al., 2017).

The Characteristic Energy Metabolism of GF Mice

To assess whether our results could be explained by antibiotic toxicity effects on thermogenesis, we used GF mice to further verify our results. The core results in GF mice were consistent with the data we obtained from ABX mice. At room temperature, GF mice had a significantly lower core body temperature (35.88°C ± 0.25°C) compared to specific-pathogen-free (SPF) mice (36.83°C ± 0.12°C) (2-tailed Mann-Whitney test, p = 0.0041) (Figure 4A) without a thermal conductance difference (1-way ANOVA, $F_{2,10}$ = 50.15, p = 0.9888) (Figure S4A). Using the doubly labeled water (DLW) technique (Speakman, 1997), we measured the energy metabolism of GF mice and found that GF mice had lower DEEs than SPF mice, despite being substantially heavier (2-tailed Mann-Whitney test, p < 0.0001). Across the SPF individuals, the body mass averaged 26.22 ± 0.27 g and DEE averaged 42.50 ± 1.24 kJ/day (n = 16). In the GF mice, the equivalent values were 34.04 ± 1.02 g and 18.61 ± 1.27 kJ/day (n = 12) (Figure 4B). Furthermore, we observed no beneficial effect of the absence of microbiota in GF mice on the browning in scWAT by either qPCR (2-way ANOVA, $F_{1,16}$ = 17.79, p > 0.9999) or western blot analysis (2-way ANOVA, $F_{1,16}$ = 12.55, p = 0.1584) compared to SPF mice (Figures 4C and 4D). These observations contrast the previous study, which suggested that GF mice have more *Ucp1* in scWAT (Suárez-Zamorano et al., 2015). We observed no significant differences in the expression profiles of markers of adipocyte differentiation or mitochondrial electron transport-related genes in the scWAT of GF mice (Figure 4C). Furthermore, the UCP1 expression in BAT was significantly reduced (~55%) (2-way ANOVA, $F_{1,16}$ = 12.55, p = 0.0307), but there was no change in the hormone-sensitive lipase levels (2-tailed Mann-Whitney test, p = 0.1508) (Figure 4D). Notably, despite the significant upregulation of IL-4 (2-tailed Mann-Whitney test, p = 0.0003), IL-5 (p = 0.0047), and IL-33 (p = 0.003) in the scWAT of GF mice, there were no differences in the expression of thermogenic genes, suggesting that type 2 cytokines are not the key drivers of the browning process in the GF model (Figure 4E). Rather, upregulation of these cytokines may be compensation for the compromised immune system of GF mice (Arpaia et al., 2013; Brestoff and Artis, 2013; Hill et al., 2012). Noradrenaline levels were also higher in the scWAT of GF mice (2-tailed Mann-Whitney test, p = 0.0648) (Figure 4E). This suggested that scWAT of GF mice was resistant to noradrenaline-induced browning. To demonstrate whether this was the case, we administrated SPF and GF mice with CL-316243 (1 mg/kg) for 2 days. The dose of CL-316243 that each GF mouse received was significantly higher than that for SPF mice based on their greater body weight, but notably, the amount of UCP1 protein in the scWAT of GF mice post-treatment was significantly lower (1-way ANOVA $F_{1,6}$ = 5.98, p = 0.04) (Figure 4F). After CL-316243 treatment, more multilocular lipid droplets adipocytes appeared in the scWAT of SPF mice than in GF mice, which is a classic "browning" phenotype (Figure 4G). The browning of WAT induced by CL-316243 increases the use of fatty acids as a metabolic substrate. The weight of scWAT (2-way ANOVA, $F_{1,20}$ = 1.092, p = 0.0212) and pgVAT (2-way ANOVA, $F_{1,20}$ = 1.648, p = 0.0032) significantly decreased in the SPF group (Figure S4B), and the content of FFA was reduced (2-way ANOVA, $F_{1,21}$ = 14.59, p = 0.0003) but not in GF mice (2-way ANOVA, $F_{1,21}$ = 14.59, p > 0.9999) (Figures 4H and S4C). Triglyceride decreased in both the SPF group (2-way ANOVA, $F_{1,21}$ = 103.5, p < 0.0001) and the GF group (2-way ANOVA, $F_{1,21}$ = 103.5, p = 0.0008). With the decrease in fat mass, leptin content was also reduced in SPF mice, but adiponectin levels were unchanged (Figure 4H). These results further support our conclusion that type 2 cytokines cannot promote the browning of scWAT. Despite higher levels of type 2 cytokines and norepinephrine, microbiota depletion did not promote the browning of scWAT in GF mice.

Figure 3. Alternatively Activated Macrophages Do Not Affect Energy Metabolism and Thermogenesis in ABX Mice

(A and B) Gene expression analysis of immune markers in BAT (A) and scWAT (B) (n = 5–8).

(C–E) Fluorescence-activated cell sorting (FACS) analysis of the cell percentages of pan-macrophage, type 2 macrophage, and eosinophil in BAT (C), scWAT (D), and pgVAT (E) under 22°C and 4°C (n = 6).

(F) Tissue type 2 cytokine levels (IL-4, IL-5, and IL-33) in scWAT, normalized to total protein concentration, under different ambient temperatures (n = 8–10).

(G) The noradrenaline level in scWAT, normalized to total protein concentration, under 22°C and 4°C (n = 8).

(H) Energy expenditure as determined by longitudinal and average oxygen consumption rates of PBS or IL-4 (50 μg/kg) treatment in control and ABX mice (n = 4) at room temperature (23°C ± 1°C).

(I) Circulating FFA, triglyceride, insulin, and leptin levels in control and ABX mice under different ambient temperatures (n = 4–9).

The results shown are representative of 2 independent experiments (A–E). All results are given as mean ± SEM and statistical analyses were performed using the Student's t test and regular one-way or two-way ANOVA. Differences with p < 0.05 were considered to be significant. *p < 0.05, **p < 0.01, ***p < 0.001, and ****p < 0.0001. See also Figure S3.

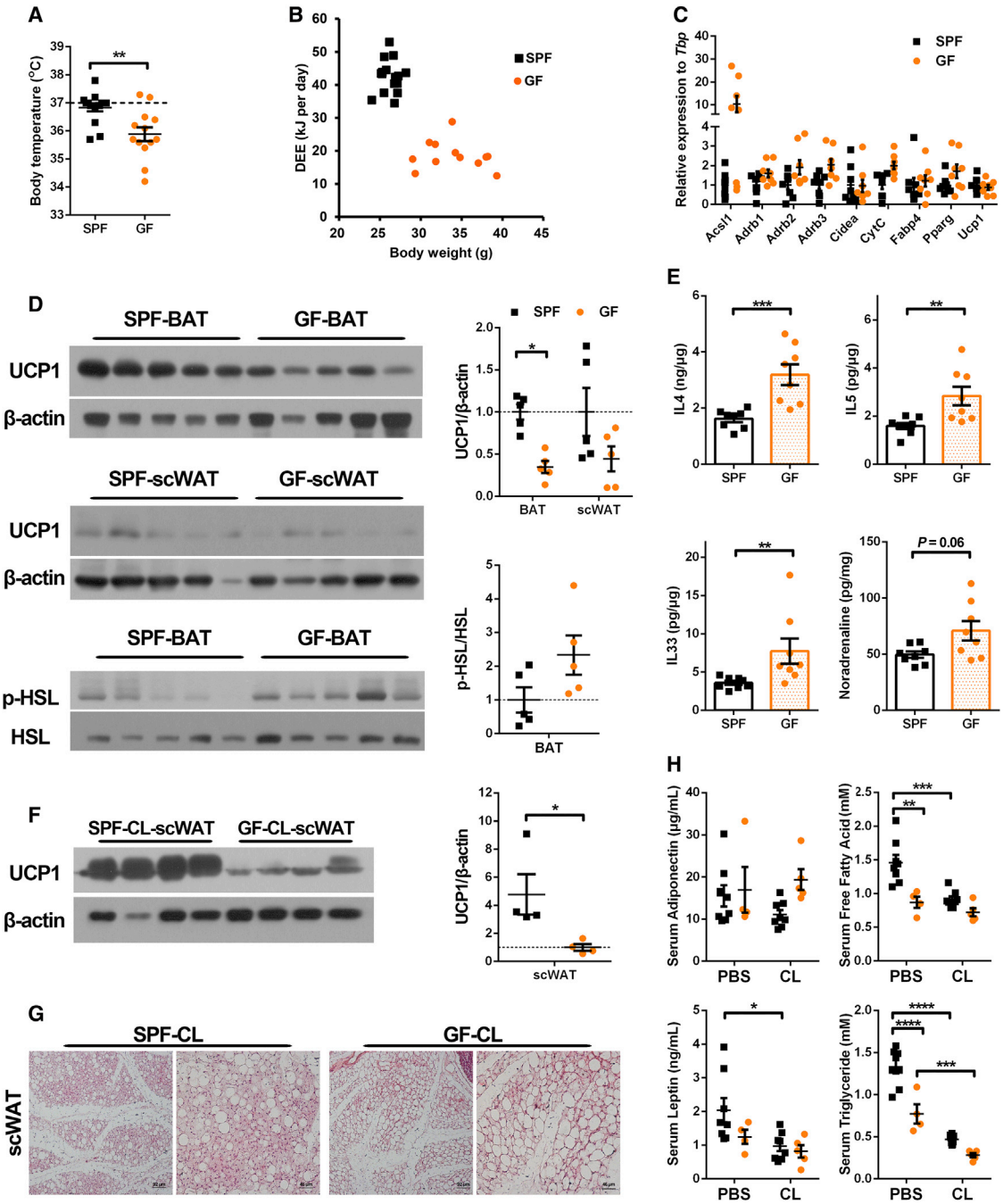

Figure 4. The Characteristic Energy Metabolism of GF Mice

(A) Rectal temperature of SPF and GF mice at room temperature (n = 13–16).

(B) DEE (kilojoules per day) using the DLW method in SPF mice (n = 16) and GF mice (n = 12) in relation to body weight (grams).

(C) Gene expression analysis of the thermogenic markers in the scWAT of SPF and GF mice (n = 8).

(D) Representative western blot and quantification of UCP1 and hormone-sensitive lipase (HSL) in the BAT and scWAT of SPF and GF mice at 22°C (n = 5).

(E) Tissue type 2 cytokine levels (IL-4, IL-5, and IL-33) and the noradrenaline level of SPF and GF mice in scWAT, normalized to total protein concentration, at 22°C (n = 8).

(F) Representative western blot and quantification of UCP1 in scWAT of SPF and GF mice treated with CL-316243 for 2 days (n = 4).

(G) H&E staining on sections from the scWAT of SPF and GF mice treated with CL-316243 for 2 days. Right image shows part of the image zoomed on the left. Scale bars: left, 92 μm; right, 46 μm.

(H) Circulating adiponectin, FFA, leptin, and triglyceride levels in SPF and GF mice treated with PBS or CL-316243 for 2 days.

All results are given as mean ± SEM and statistical analyses were performed using the Student's t test and regular one-way or two-way ANOVA. Differences with $p < 0.05$ were considered to be significant. *$p < 0.05$, **$p < 0.01$, ***$p < 0.001$, and ****$p < 0.0001$. See also Figure S4.

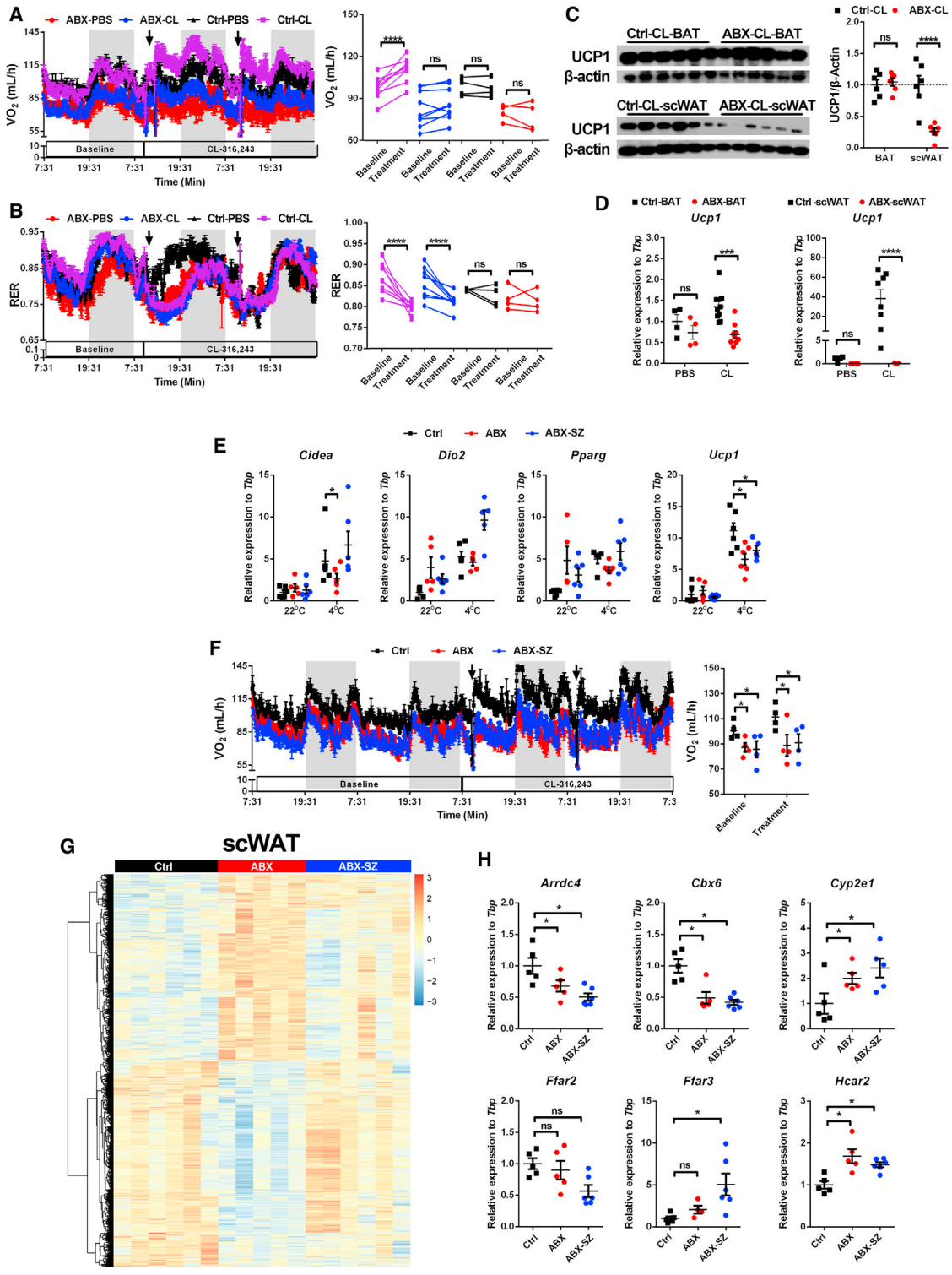

Figure 5. Depletion of the Microbiota by Different Antibiotic Cocktail Protocols Have Similar Physiological Effects

(A and B) Energy expenditure as determined by longitudinal and average oxygen consumption rate (A) and RER (B) before and after PBS (n = 4 per group) or CL-316243 (n = 8 per group) treatment in control and ABX mice.

(C) Representative western blot and quantification of UCP1 in the BAT and scWAT from the control group and the ABX group after CL-316243 treatment for 2 days (n = 6).

(D) Gene expression analysis of *Ucp1* in the BAT and scWAT of control and ABX mice (n = 4 in PBS group and n = 9 in CL-316243 treatment group).

(legend continued on next page)

Depletion of the Microbiota by Different ABX Protocols Have Similar Physiological Effects

We explored whether ABX affected β3-adrenoceptor activation. Oxygen consumption in response to CL-316243 at room temperature was significantly and rapidly elevated in control mice compared to PBS treatment (2-way ANOVA, $F_{22,22}$ = 12.39, $p < 0.0001$). However, this induction was severely attenuated in ABX mice (2-way ANOVA, $F_{22,22}$ = 12.39, p = 0.2178) (Figure 5A). There was no difference in the RER (2-way ANOVA, $F_{22,22}$ = 1.256, $p > 0.9999$) (Figure 5B) or physical activity (2-way ANOVA, $F_{22,22}$ = 7.588, $p > 0.9999$) (Figure S5A) between control and ABX mice under CL-316243 treatment. Nevertheless, control mice gained significantly more UCP1 protein (2-way ANOVA, $F_{1,20}$ = 13.37, $p < 0.0001$) (Figure 5C) and *Ucp1* mRNA (2-way ANOVA, $F_{1,21}$ = 9.244, $p < 0.0001$) in scWAT (Figure 5D) under CL-316243 treatment than ABX mice did.

We next asked whether different ABX formulations could also suppress thermogenesis. We repeated our ABX experiment along with another published ABX protocol (referred to here as ABX-SZ) for 30 days. Both ABX and ABX-SZ demonstrated no difference in body weight (2-way repeated-measures ANOVA, $F_{21,588}$ = 105.1, p = 0.3635) and food intake (2-way repeated-measures ANOVA, $F_{21,567}$ = 9.962, p = 0.7) compared to control mice after 30 days' treatment (Figures S5B and S5C), and they demonstrated no difference in tissue mass at different anatomic sites between ABX and ABX-SZ (Figure S5D). Compared to control mice, both ABX and ABX-SZ mice had similar *Ucp1* gene expression levels in scWAT at room temperature (2-way ANOVA, $F_{1,28}$ = 103.4, $p > 0.9999$), but *Ucp1* gene expression level was significantly decreased when acutely exposed to an ambient temperature of 4°C for 48 h (2-way ANOVA, $F_{1,28}$ = 103.4, p = 0.0010) (Figure 5E). There was no difference between ABX and ABX-SZ in oxygen consumption (2-way ANOVA, $F_{2,9}$ = 3.23, $p > 0.9999$), RER (2-way ANOVA, $F_{2,9}$ = 2.887, p = 0.1583), and physical activity (2-way ANOVA, $F_{2,9}$ = 3.835, p = 0.0784) before and after CL-316243 treatment at room temperature (Figures 5F, S5E, and S5F). Compared to control mice, both ABX and ABX-SZ mice showed lower oxygen consumption (2-way ANOVA, $F_{2,9}$ = 13.43, p = 0.0313) after CL-316243 treatment. There was also no difference in RER (2-way ANOVA, $F_{2,9}$ = 2.887, $p > 0.9999$) and physical activity (2-way ANOVA, $F_{2,9}$ = 3.980, $p > 0.9999$) in ABX-SZ mice compared to control mice.

To determine the gene expression signatures after different ABX treatments in fat tissue, we performed RNA-seq analysis in scWAT and pgVAT from mice at room temperature on treatment day 28. Hierarchical clustering of the differentially expressed genes among the RNA-seq samples is shown in Figures 5G, S6A, and S6B, and Table S2. The main differences in scWAT were related to immune pathways, and no difference was found in pgVAT between ABX and ABX-SZ (Figure S6D). Consistent with our qPCR results, both ABX and ABX-SZ mice showed no differences in the gene expression of *Ucp1*, M2 markers, or type 2 cytokines compared to control mice. The butyrate receptor *Hcar2* (hydroxycarboxylic acid receptor 2, also known as *Gpr109a*) was significantly upregulated in both ABX and ABX-SZ mice compared to control mice, while the FFA receptors *Ffar2* (also known as *Gpr43*) and *Ffar3* (also known as *Gpr41*) showed no difference (Figure S6C). Selected gene expression was validated by qPCR (Figure 5H**)**. There was no difference in gene expression pattern between ABX and ABX-SZ in pgVAT (Table S3). Our data suggested that the depletion of the microbiota by different ABX protocols had similar effects and did not promote elevated DEE and adaptive thermogenesis.

Recolonization Microbiota and Butyrate Partially Rescue the Thermogenesis of ABX Mice

We assessed 16S rDNA contents per the fecal pellet in control, ABX, and ABX-SZ mice by qPCR (Thackray et al., 2018). Both ABX and ABX-SZ treatments reduced bacterial contents to $(5 \pm 0.5) \times 10^4$ pg DNA per gram fecal pellet compared to $(2.8 \pm 0.2) \times 10^7$ pg/g in control mice. These changes took place immediately after the ABX and ABX-SZ treatments, suggesting that both ABX protocols efficiently depleted the majority of gut microbiota (Figure 6A). Sequencing of 16S rDNA amplicons from the cecum revealed that fewer operational taxonomic units (OTUs) were detected from ABX and ABX-SZ groups compared to the control group (Figure 6B). Furthermore, weighted unique fraction metric (UniFrac) principal-coordinate analysis (PCoA) illustrated that these 2 different antibiotic protocol treatments (ABX and ABX-SZ) had similar impacts on the bacterial composition (Figure 6C). *Lachnospiraceae* (belonging to the butyrate-producing bacteria *Clostridia*) were induced by cold stimulation in control mice (Figures 6D, 6E, S7A, and S7B). PF individuals that showed a higher *Ucp1* expression level also had significantly higher *Clostridia*. The DNA abundance of *Clostridia* in the remaining ABX and ABX-SZ feces contents were significantly lower than in control mice at 4°C.

We explored whether the repopulation of microbiota in ABX mice could reverse the negative impact on WAT browning. Immediately following the withdrawal of antibiotic treatment, ABX mice were transferred to cages containing the old nests and dirty bedding of control mice for 5 days. After 5 days of

(E) Gene expression analysis of the thermogenic markers in the scWAT of control, ABX, and ABX-SZ mice (n = 5–6).
(F) Energy expenditure as determined by longitudinal and average oxygen consumption rates before and after CL-316243 (n = 4 per group) treatment in control, ABX, and ABX-SZ mice.
(G) Hierarchical clustering of the differentially expressed genes from the sequencing dataset in scWAT (n = 5–6). Rows were clustered using the one minus Pearson correlation distance metric, and columns were clustered using the one minus Spearman correlation distance metric. Clustering was performed with the averaged counts for each cell type.
(H) Highlighted differentially expressed genes validated by qPCR from the ABX and ABX-SZ groups compared to the control group in the RNA sequencing dataset.
The results shown are representative of 2 independent experiments (A–F). All results are given as mean ± SEM and statistical analyses were performed using the Student's t test and regular one-way or two-way ANOVA. Differences with $p < 0.05$ were considered to be significant. *$p < 0.05$, **$p < 0.01$, ***$p < 0.001$, and ****$p < 0.0001$. See also Figures S5 and S6 and Tables S2 and S3.

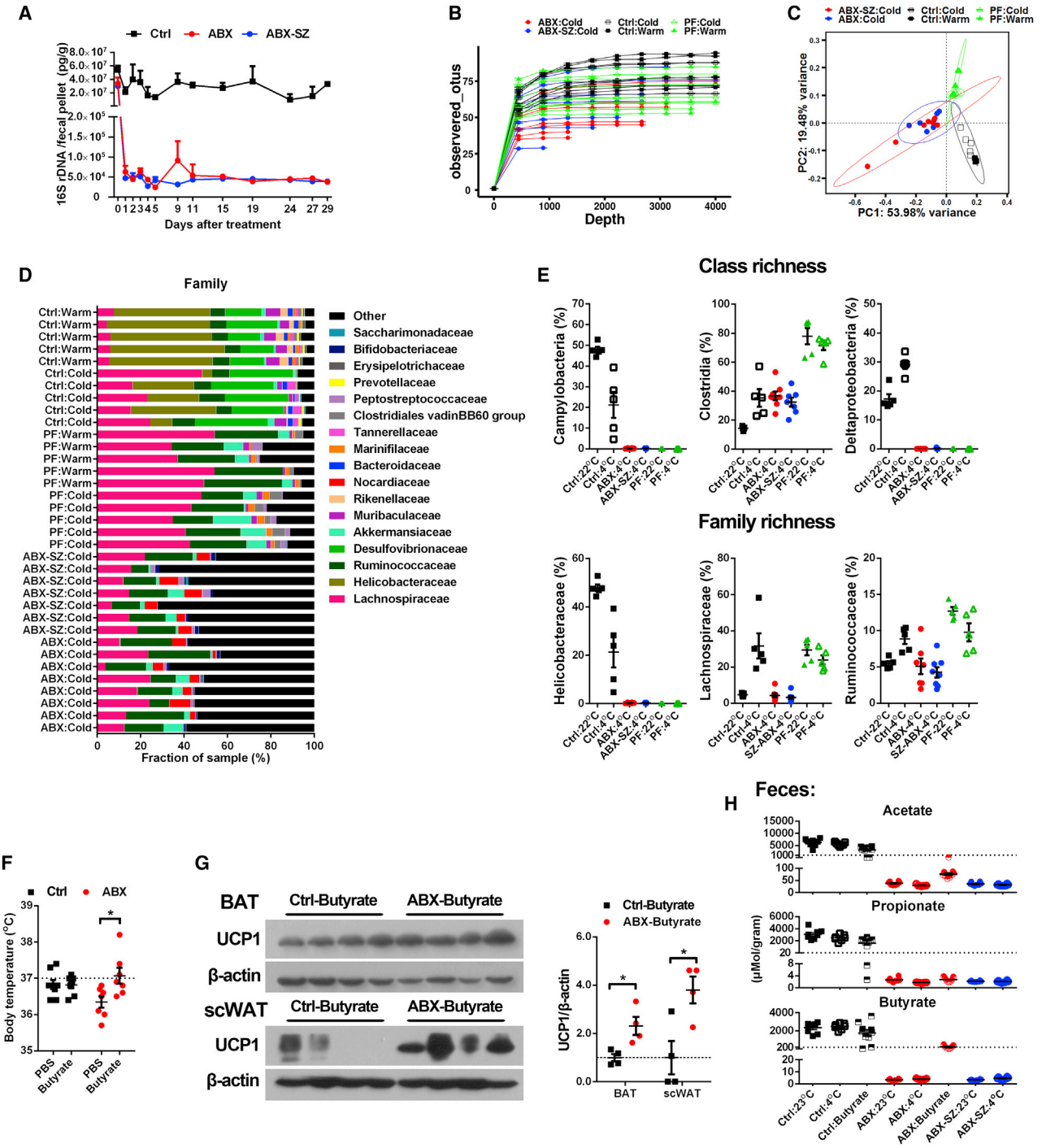

Figure 6. Recolonization Microbiota and Butyrate Partially Rescue the Thermogenesis of ABX Mice

(A) Bacterial 16S rDNA content per gram feces from treatment days 0–29 were determined by qPCR (n = 3 per group).

(B) Observed OTUs (99% similarity) in cecum feces (n = 5–8).

(C) Weighted UniFrac PCoA of the cecum microbiota.

(D) Comparison of the family-level proportional abundance of cecum feces.

(E) Richness represented as the proportions of OTUs classified at the class and family ranks (n = 5–8).

(F) The changes of rectal temperature of control and ABX mice after PBS or butyrate treatment for 7 days at room temperature (23°C ± 1°C) (n = 8 in the control group and n = 7 in the ABX group).

(legend continued on next page)

microbiota repopulation treatment, these mice were transferred into an ambient temperature of 4°C for 48 h. We found that the 16S rDNA contents per fecal pellet measured by qPCR (Thackray et al., 2018) and the short-chain fatty acid (SCFA) levels, including acetate, propionate, and butyrate from the cecum feces, were significantly restored in the repopulated mice (RO) compared to the ABX mice (Figures S7C and S7D). RO mice had a significantly increased expression of *Ucp1* (1-way ANOVA, $F_{2,13} = 8.492$, $p = 0.0036$) in response to cold stimulation compared to ABX mice (Iida et al., 2013) (Figure S7E). These data indicated that gut microbiota recolonization benefits adaptive thermogenesis in scWAT.

A potential mechanism by which microbiota may influence host metabolism is via metabolites generated during microbial fermentation in the gut. Previous studies reported that commensal bacterial metabolites SCFAs, especially butyrate, a typical histone deacetylase (HDAC) inhibitor (Candido et al., 1978; Sealy and Chalkley, 1978), may regulate the expression of numerous genes through different mechanisms (Arpaia et al., 2013; Ganal et al., 2012; Kaiko et al., 2016; Mariño et al., 2017; Olszak et al., 2012; Walsh et al., 2015). HDAC1 and HDAC3 have been demonstrated to play a key role in the thermogenesis process (Emmett et al., 2017; Li et al., 2016). Most of the butyrate in the cecum may be used by mitochondria as the energy substrate in the colon. However, some butyrate could enter the circulation system and cross the blood-brain barrier via monocarboxylate transporters (MCTs) (Vijay and Morris, 2014). Recent studies suggested that butyrate could activate BAT via a direct gut-brain neural circuit (Li et al., 2018). We therefore assessed whether exogenous butyrate would promote the adaptive thermogenesis in mice with depleted microbiota. Both control and ABX mice were administered butyrate sodium (80 mg/day) for a consecutive 7 days by oral gavage at room temperature (23°C ± 1°C). We found that the core body temperature of ABX mice increased from 36.34°C ± 0.16°C to 37.07°C ± 0.22°C (2-way ANOVA, $F_{1,26} = 0.5477$, $p = 0.0165$), but there was no significant effect on control mice (from 36.83°C ± 0.13°C to 36.82°C ± 0.09°C) (Figure 6F). Protein analysis showed that butyrate treatment significantly increased UCP1 content in BAT (1-way ANOVA, $F_{1,6} = 5.98$, $p = 0.017$) and scWAT (1-way ANOVA, $F_{1,6} = 5.98$, $p = 0.019$) of ABX mice compared to control mice (Figure 6G), but butyrate treatment had no influence on body weight in control and ABX mice (Figure S7F). A recent study suggested that butyrate decreases food intake and inhibits orexigenic neuron activity in the hypothalamus (Li et al., 2018). We also found that butyrate decreased food intake in the control group, but not in the ABX-treated group (Figure S7G). The butyrate level in the cecum feces was significantly decreased by a factor of ~1,000 in ABX (3.4 ± 0.2 μMol/g) and ABX-SZ (3.2 ± 0.14 μMol/g) individuals. The butyrate gavage treatment restored an ~10% butyrate level (220.2 ± 54.6 μMol/g) compared to the control group (2,352 ± 206.2 μMol/g) (Figure 6H). In contrast to the cecum feces, there was no significant difference between control mice and ABX mice in the serum butyrate levels after butyrate gavage. This result is consistent with recent studies that indicated that the suppression of food intake by butyrate gavage was independent of the circulating butyrate levels (Chevalier et al., 2015; Li et al., 2018) (Figure S7H; Table S4). These data suggest that the bacterial metabolite butyrate increased the energy expenditure and partially rescued the impaired thermogenesis induced by the depletion of microbiota.

Isotope Tracing and ^{13}C-Butyrate Metabolic Flux Analysis *In Vivo*

The mechanism by which butyrate may regulate body temperature and UCP1 expression is not clear. One possible mechanism is that oral-gavaged butyrate could be distributed to peripheral tissues, such as BAT and WAT, when the microbiota is depleted and the butyrate plays the role of an energy substrate or an HDAC inhibitor. An alternative possible mechanism is that the brain is sensitized to gut butyrate levels after ABX treatment, and the gavaged butyrate regulates BAT through an activated gut-brain axis. To explore these different mechanisms, we measured whether there was a difference in exogenous butyrate distribution using gavage of ^{13}C-labeled butyrate. We administrated the same level of butyrate sodium to control and ABX mice for 6 days and gavage mixed [U^{13}C] and ^{12}C butyrate sodium (1:9 ratio) at day 7. Butyrate could be used by mitochondria after distribution and exhaled as CO_2. We therefore carefully determined the time of sacrifice at 1 h after gavage by measuring the $^{13}CO_2$ in control mice (Figure S8A). Since butyrate could enter the tricarboxylic acid (TCA) cycle via acetyl-coenzyme A (CoA), we performed a targeted metabolite analysis for SCFA and TCA metabolites in several tissues (Figure 7A). The uptake of acetate, propionate, and butyrate in the cecum and colon were largely limited in ABX individuals, and the butyrate gavage treatment could selectively restore butyrate levels in the cecum and colon (Figures 7B, 7C, S8B, and S8C). The ^{13}C:^{12}C ratio of butyrate in ABX individuals was significantly higher than that in control individuals in the colon (7.8% ± 1.1% versus 10.5% ± 0.4%) and cecum (7.6% ± 1.1% versus 10.4% ± 0.4%) (Figure 7F). We found that several $m + 2$ isotopologues of TCA metabolites such as citrate, succinate, fumarate, and malate were significantly enriched in the brains of ABX mice compared to control mice after butyrate gavage treatment (Figure 7D). More important, the fractional contribution of [U^{13}C] butyrate to citrate was substantially higher in the brain (>1:9 ratio) than BAT, scWAT, colon, and cecum, and the ^{13}C:^{12}C ratio of citrate was significantly higher in ABX individuals (42.2% ± 4.5%) compared to control individuals (25.3% ± 3.3%) in the brain (Figure 7F). This result suggested that there is a selective route for butyrate from the gut to the brain. Recent studies suggested that the enrichment of succinate could activate thermogenesis in BAT (Mills

(G) Representative western blot and quantification of UCP1 in the BAT and scWAT of control and ABX mice after PBS or butyrate treatment for 7 days.
(H) SCFA levels per gram feces in the cecum (n = 6–8 per group).
All results are given as mean ± SEM and statistical analyses were performed using the Student's t test and regular one-way or two-way ANOVA. Differences with $p < 0.05$ were considered to be significant. *$p < 0.05$, **$p < 0.01$, ***$p < 0.001$, and ****$p < 0.0001$. See also Figure S7 and Table S4.

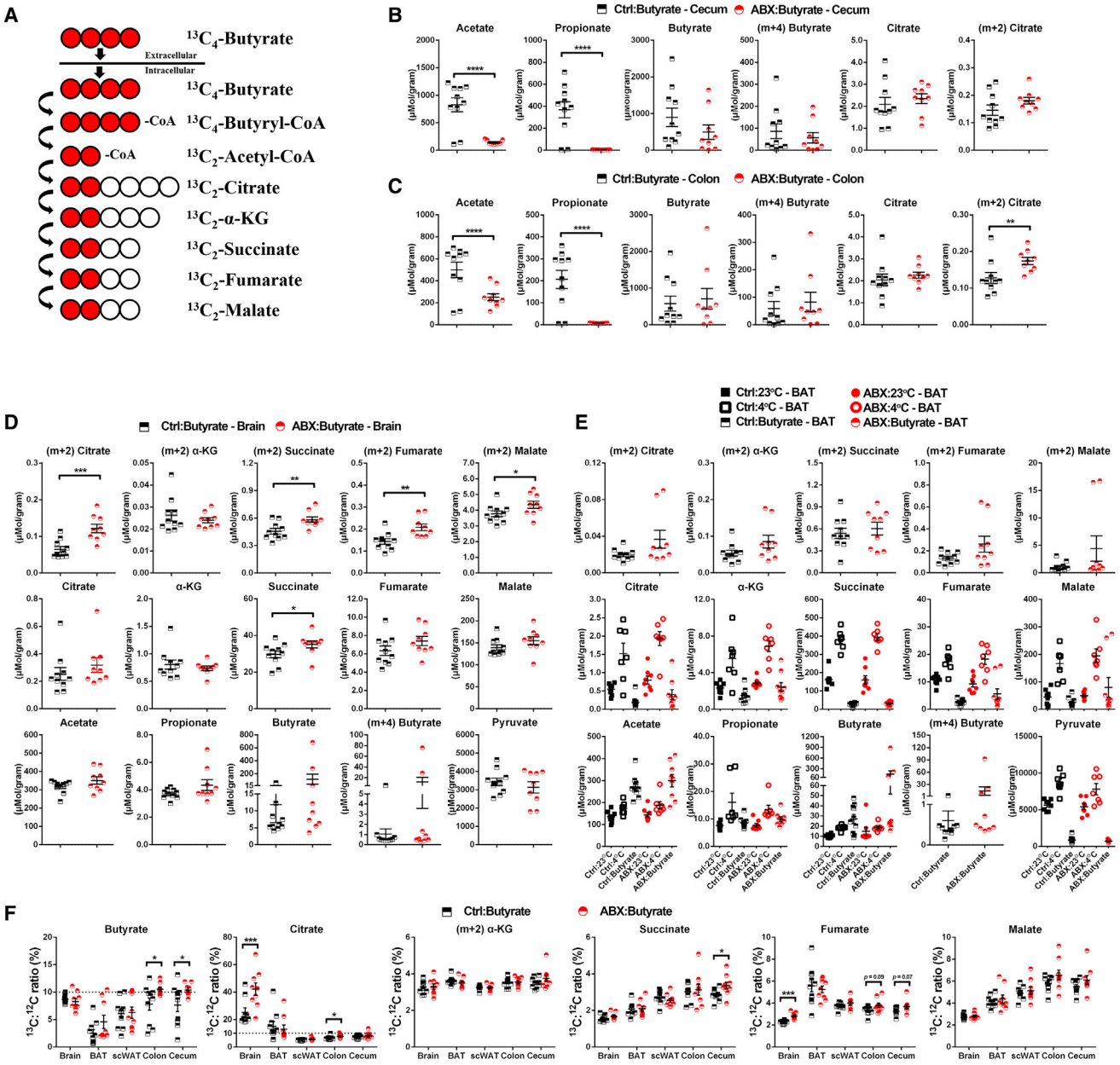

Figure 7. Isotope Tracing and ^{13}C-Butyrate Metabolic Flux Analysis *In Vivo*

(A) Schematic diagrams of ^{13}C-butyrate tracing experiments in mice.

(B–E) Abundance of isotopic labeling TCA cycle metabolites and SCFA in cecum (B), colon (C), brain (D), and BAT (E) (n = 6–10).

(F) Proportional isotopic labeling profiles of TCA cycle metabolites (n = 9–10).

Data represent means ± SEMs, based on 2-tailed Mann-Whitney test (F). All results are given as mean ± SEM and statistical analyses were performed using the Student's t test and regular one-way or two-way ANOVA. Differences with $p < 0.05$ were considered to be significant. *$p < 0.05$, **$p < 0.01$, ***$p < 0.001$, and ****$p < 0.0001$. See also Figure S8.

et al., 2018), and we confirmed that the succinate levels were higher than other TCA metabolites in the cold-stimulated BAT (Figure 7E). There was no significant enrichment difference in *m* + 4 butyrate or *m* + 2 TCA metabolites in BAT (Figure 7E) and scWAT (Figures S8D and S8E) between control and ABX mice after butyrate gavage treatment. These results indicated that butyrate probably regulates body temperature and UCP1 expression via an activated gut-brain axis, rather than by a direct interaction between butyrate and the adipose tissues.

DISCUSSION

Increasing numbers of studies have reported relations between the gut microbiota and physiological states of the host in both

mice and humans. Although some studies indicated a link between the gut microbiota and obesity and diabetes (Cani et al., 2012; Cox and Blaser, 2013; Ley et al., 2005; Turnbaugh et al., 2006), the impact of the gut microbiota on different adipocytes is unclear. Since UCP1 plays a vital role in nonshivering thermogenesis, we focused on whether the gut microbiota affects UCP1-dependent thermogenesis. We found that UCP1 was blunted during an acute cold ambient temperature challenge and after administration of a β3-adrenoceptor (Adrb3) agonist, when the gut microbiota was absent. Our work supports the idea of a link between gut microbiota and UCP1-dependent thermogenesis of brown and beige (brite) adipocytes. Increasing evidence suggests that UCP1 is not required in long-term cold adaptation, and the glucose uptake of BAT under CL-316243 stimulation (Keipert et al., 2017) and UCP1-independent thermogenic mechanisms such as creatine (Kazak et al., 2015) or sarcoplasmic/endoplasmic reticulum Ca^{2+}-ATPase 2b (SERCA2b) (Ikeda et al., 2017) cycles in beige adipocytes may also contribute to whole-body energy homeostasis. Whether these processes are also impaired in the absence of the gut microbiota is currently unknown.

GF and ABX mice have been used frequently to study the impact of gut microbiota on the host (Lundberg et al., 2016; Sivan et al., 2015; Vétizou et al., 2015; Yang et al., 2017). Here, we reported some physiological characteristics of ABX and GF mice, including the measurement of DEE of GF animals using the DLW technique, and β3-adrenergic-induced thermogenesis. Many previous studies reported that ABX or GF mice resist high-fat diet-induced obesity and have improved glucose metabolism (Bäckhed et al., 2004; Chevalier et al., 2015; Zarrinpar et al., 2018). We found that UCP1 expression and whole-body energy expenditure were blunted with the depletion of gut microbiota. This contrasts a previous study (Suárez-Zamorano et al., 2015), which suggested that microbiota depletion promotes browning. The mix of antibiotics that they used differed from what we used. Accordingly, we replicated our studies using their antibiotic recipe (ABX-SZ) but did not find that microbiota depletion facilitated the browning of WAT. In contrast, we found that antibiotic-treated mice (independent of the cocktail used) and GF mice had an impaired capacity for UCP1-dependent thermogenesis. In addition, the downregulated UCP1 expression we observed may be considered to be inconsistent with the improved glucose metabolism performance in the ABX mice. However, the capacity for glucose uptake is not always positively correlated with UCP1-dependent thermogenesis (Olsen et al., 2017). For example, recent studies suggested that glucose uptake is elevated in Ucp1-knockout (KO) mice and that brown or beige adipocytes could consume glucose via the SERCA2b pathway in an UCP1-independent manner (Ikeda et al., 2017; Olsen et al., 2017).

A healthy gut microbiota community benefits host metabolic homeostasis, and reciprocally, gut microbiota composition can be shaped by ambient temperature and macronutrients from the diet (Chevalier et al., 2015; Dey et al., 2015; Kau et al., 2011; Turnbaugh et al., 2008; Ziętak et al., 2016). It has been suggested that SCFA levels are positively associated with enhanced energy metabolism (Donohoe et al., 2011; Gao et al., 2009; Li et al., 2018), while other microbiota-derived metabolites such as trimethylamine and imidazole propionate were suggested to be negatively linked to host health (Hsiao et al., 2013; Koeth et al., 2013; Koh et al., 2018). The microbiota-derived metabolites not only play vital roles in host immune education and pathogen defense but are also involved in host nutrition status (Blanton et al., 2016; Guglielmi, 2018). Here, we confirmed that the energy absorption capacity declined in ABX mice; furthermore, the PF mice results suggested that energy intake and the temporarily lowered body weight observed in ABX mice were not the cause for the lower energy expenditure and the dampened thermogenic capacity. The absence of gut microbiota, via antibiotic treatment or in the GF model, can result in a depletion of metabolites generated during microbial fermentation in the gut, thereby promoting a state of gut metabolite deficiency. Our results are consistent with previous studies that showed that under ABX treatment, all types of SCFAs and bile acids almost disappeared in the cecum. A previous study showed that butyrate-producing bacteria were increased by cold stimulation (Chevalier et al., 2015), and we confirmed this phenotype. The expression of *Hcar2,* a butyrate receptor (Offermanns, 2017), was dramatically increased in both ABX and ABX-SZ mice compared to control mice, while other SCFA receptors *Ffar2* and *Ffar3* showed no difference. Several recent studies suggested that exogenous butyrate could enhance host energy expenditure and promote UCP1 expression (Gao et al., 2009; Li et al., 2018). In a pilot study, we also found that exogenous butyrate had larger effects than acetate and propionate (data not shown). This led us to assess whether exogenous butyrate could rescue hypothermia and promote UCP1 expression when the gut microbiota was absent. Using ^{13}C-butyrate metabolic flux analysis, we found that butyrate uptake and utilization were faster in brain than in BAT and WAT once butyrate enters the circulation. This suggests that butyrate possibly acts in the brain via the gut-brain axis (Mayer et al., 2015) to regulate food intake and thermogenesis.

In summary, these data showed that antibiotic-mediated depletion of microbiota does not promote browning of WAT through type 2 cytokine signaling and alternatively activated macrophages, but rather negatively affects adaptive thermogenesis mediated via both interscapular BAT and the browning of scWAT. These effects were confirmed in GF mice and in mice treated with a different ABX. An intact microbiota may thus be an essential component of the thermoregulatory response, and microbial-derived butyrate may be a mediating factor in this role.

LIMITATIONS OF STUDY

Although we found that DEE and UCP1-dependent thermogenesis were blunted via two common ABX protocols and in GF mice (Abt et al., 2012; Suárez-Zamorano et al., 2015), our work has several limitations. First, it is inevitable that the background of gut microbiota composition from our work is distinct from other studies because of different housing conditions, diet, sex, age, antibiotic administration route (drinking water or gavage), and other factors (Ussar et al., 2015). This is a major challenge for the repeatability in gut microbiota studies. Furthermore, several antibiotics have been reported to be toxic to mitochondria (Hangas et al., 2018; Jiang et al., 2018; Kalghatgi et al.,

2013; Moullan et al., 2015). It is possible that the mitochondrial function of the host was affected by the antibiotics, even though we obtained the same results using two rather different cocktails. However, we also successfully replicated some of the data using GF mice, in which no such antibiotic artifacts would be present. Nevertheless, a gold standard procedure for antibiotic treatment mice is urgently needed for gut microbiota research. Alternatively, studies should use, as we have, multiple cocktails of antibiotics to show that the response is not cocktail dependent.

Second, the gut microbiota composition is complex, and even multiple combinations of antibiotics are unable to deplete the gut microbiota completely. Antibiotic-resistant bacteria and fungi remain in the tract under ABX treatment; hence, it is possible that the imbalance of gut microbiota could influence host energy homeostasis (Dollive et al., 2013; Lopez et al., 2014; Underhill and Iliev, 2014). Our study clearly showed that the composition was changed under cold challenge. However, we were not able to isolate the impact of the gut microbiome to a single species in the microbiota. This may not be a single species effect, and the details of this mechanism require more study.

Third, the molecular mechanism underlying the role of butyrate inducing thermogenesis in ABX mice remains unclear. Our data showed that the butyrate receptor *Hcar2* was increased in ABX mice, suggesting that they may be more sensitive to exogenous butyrate. Then, the molecular function of butyrate on thermogenesis may be related to its role as HDAC inhibitor (Emmett et al., 2017; Li et al., 2016; Walsh et al., 2015). Using ^{13}C-butyrate metabolic flux analysis, we showed that the brain uptakes and uses more butyrate than both BAT and WAT. This is consistent with a recent report (Li et al., 2018) suggesting that butyrate could activate BAT through the gut-brain neural circuit. More work is needed to explore the function of butyrate on the brain.

Lastly, we found that both 3- to 4-week treated ABX and GF mice showed hypothermia and attenuated energy expenditure after administering a β3-adrenoceptor agonist. However, we were unable to perform a cold challenge on GF mice because of their special housing conditions. Not all experiments are feasible for GF mice, which is a common drawback of their use. Despite these limitations, our study still provides the clear relation between gut microbiota and adaptive thermogenesis and offers some important insights into future studies using ABX and GF mouse models to further investigate the mechanisms underpinning the gut-brain axis.

STAR★METHODS

Detailed methods are provided in the online version of this paper and include the following:

- KEY RESOURCES TABLE
- CONTACT FOR REAGENT AND RESOURCE SHARING
- EXPERIMENTAL MODEL AND SUBJECT DETAILS
- METHOD DETAILS
  - Metabolic phenotype analysis
  - Quantitative PCR
  - Western blotting
  - Histology
  - Hormone measurements
  - ^{13}C enrichment in breath samples
  - Quantitative analysis of SCFA and TCA cycle metabolites
  - Serum metabolites
  - RNA-seq and Bioinformatics
  - 16S rDNA qPCR and Amplicon Sequencing
  - Flow cytometry
  - Thermal conductance of pelage
- QUANTIFICATION AND STATISTICAL ANALYSIS
- DATA AND SOFTWARE AVAILABILITY

SUPPLEMENTAL INFORMATION

Supplemental Information can be found with this article online at https://doi.org/10.1016/j.celrep.2019.02.015.

ACKNOWLEDGMENTS

This work was supported by the Strategic Priority Research Program of the Chinese Academy of Sciences (XDB13030000) and Natural Science Foundation of China (NSFC; 91649108), the Chinese Academy of Sciences-Novo Nordisk Foundation, as well as grants from the Chinese Academy of Sciences "1000 Talents" recruitment program and a "Great-Wall Professorship" from the Chinese Academy of Sciences-Novo Nordisk Foundation. J.R.S. was also supported by a Wolfson merit professorship from The UK Royal Society. We are grateful to all of the members of the Molecular Energetics Group for their support and discussion of the results. We would like to thank Dr. Jia and Dr. Sun from the Core Facility for Protein Research from the Institute of Biophysics, Chinese Academy of Sciences for flow cytometry, and Peter Thomson and Marina Samatiou for technical assistance with the DLW measurements.

AUTHOR CONTRIBUTIONS

Conceptualization, J.R.S. and B.L.; Methodology, B.L., L.L., C.H., and S.M.L.; Investigation, B.L., L.L., M.L., Y.W., C.N., G.W., X.L., H.Z., W.J., C.H., S.M.L., and G.S.; Writing, L.L., B.L., and J.R.S.; Supervision, J.R.S.

DECLARATION OF INTERESTS

The authors declare no competing interests.

Received: November 2, 2018
Revised: January 9, 2019
Accepted: February 2, 2019
Published: March 5, 2019

REFERENCES

Abt, M.C., Osborne, L.C., Monticelli, L.A., Doering, T.A., Alenghat, T., Sonnenberg, G.F., Paley, M.A., Antenus, M., Williams, K.L., Erikson, J., et al. (2012). Commensal bacteria calibrate the activation threshold of innate antiviral immunity. Immunity *37*, 158–170.

Arpaia, N., Campbell, C., Fan, X., Dikiy, S., van der Veeken, J., deRoos, P., Liu, H., Cross, J.R., Pfeffer, K., Coffer, P.J., and Rudensky, A.Y. (2013). Metabolites produced by commensal bacteria promote peripheral regulatory T-cell generation. Nature *504*, 451–455.

Bäckhed, F., Ding, H., Wang, T., Hooper, L.V., Koh, G.Y., Nagy, A., Semenkovich, C.F., and Gordon, J.I. (2004). The gut microbiota as an environmental factor that regulates fat storage. Proc. Natl. Acad. Sci. USA *101*, 15718–15723.

Blanton, L.V., Barratt, M.J., Charbonneau, M.R., Ahmed, T., and Gordon, J.I. (2016). Childhood undernutrition, the gut microbiota, and microbiota-directed therapeutics. Science *352*, 1533.

Brestoff, J.R., and Artis, D. (2013). Commensal bacteria at the interface of host metabolism and the immune system. Nat. Immunol. *14*, 676–684.

Candido, E.P., Reeves, R., and Davie, J.R. (1978). Sodium butyrate inhibits histone deacetylation in cultured cells. Cell *14*, 105–113.

Cani, P.D., Osto, M., Geurts, L., and Everard, A. (2012). Involvement of gut microbiota in the development of low-grade inflammation and type 2 diabetes associated with obesity. Gut Microbes *3*, 279–288.

Cannon, B., and Nedergaard, J. (2004). Brown adipose tissue: function and physiological significance. Physiol. Rev. *84*, 277–359.

Chevalier, C., Stojanović, O., Colin, D.J., Suarez-Zamorano, N., Tarallo, V., Veyrat-Durebex, C., Rigo, D., Fabbiano, S., Stevanović, A., Hagemann, S., et al. (2015). Gut Microbiota Orchestrates Energy Homeostasis during Cold. Cell *163*, 1360–1374.

Corp, N., Gorman, M.L., and Speakman, J.R. (1997). Seasonal variation in the resting metabolic rate of male wood mice Apodemus sylvaticus from two contrasting habitats 15 km apart. J. Comp. Physiol. B *167*, 229–239.

Cox, L.M., and Blaser, M.J. (2013). Pathways in microbe-induced obesity. Cell Metab. *17*, 883–894.

Cypess, A.M., Lehman, S., Williams, G., Tal, I., Rodman, D., Goldfine, A.B., Kuo, F.C., Palmer, E.L., Tseng, Y.H., Doria, A., et al. (2009). Identification and importance of brown adipose tissue in adult humans. N. Engl. J. Med. *360*, 1509–1517.

den Besten, G., van Eunen, K., Groen, A.K., Venema, K., Reijngoud, D.J., and Bakker, B.M. (2013). The role of short-chain fatty acids in the interplay between diet, gut microbiota, and host energy metabolism. J. Lipid Res. *54*, 2325–2340.

Dey, N., Wagner, V.E., Blanton, L.V., Cheng, J., Fontana, L., Haque, R., Ahmed, T., and Gordon, J.I. (2015). Regulators of gut motility revealed by a gnotobiotic model of diet-microbiome interactions related to travel. Cell *163*, 95–107.

Dollive, S., Chen, Y.Y., Grunberg, S., Bittinger, K., Hoffmann, C., Vandivier, L., Cuff, C., Lewis, J.D., Wu, G.D., and Bushman, F.D. (2013). Fungi of the murine gut: episodic variation and proliferation during antibiotic treatment. PLoS One *8*, e71806.

Donohoe, D.R., Garge, N., Zhang, X., Sun, W., O'Connell, T.M., Bunger, M.K., and Bultman, S.J. (2011). The microbiome and butyrate regulate energy metabolism and autophagy in the mammalian colon. Cell Metab. *13*, 517–526.

Emmett, M.J., Lim, H.W., Jager, J., Richter, H.J., Adlanmerini, M., Peed, L.C., Briggs, E.R., Steger, D.J., Ma, T., Sims, C.A., et al. (2017). Histone deacetylase 3 prepares brown adipose tissue for acute thermogenic challenge. Nature *546*, 544–548.

Fischer, K., Ruiz, H.H., Jhun, K., Finan, B., Oberlin, D.J., van der Heide, V., Kalinovich, A.V., Petrovic, N., Wolf, Y., Clemmensen, C., et al. (2017). Alternatively activated macrophages do not synthesize catecholamines or contribute to adipose tissue adaptive thermogenesis. Nat. Med. *23*, 623–630.

Flint, H.J., Scott, K.P., Louis, P., and Duncan, S.H. (2012). The role of the gut microbiota in nutrition and health. Nat. Rev. Gastroenterol. Hepatol. *9*, 577–589.

Ganal, S.C., Sanos, S.L., Kallfass, C., Oberle, K., Johner, C., Kirschning, C., Lienenklaus, S., Weiss, S., Staeheli, P., Aichele, P., and Diefenbach, A. (2012). Priming of natural killer cells by nonmucosal mononuclear phagocytes requires instructive signals from commensal microbiota. Immunity *37*, 171–186.

Gao, Z., Yin, J., Zhang, J., Ward, R.E., Martin, R.J., Lefevre, M., Cefalu, W.T., and Ye, J. (2009). Butyrate improves insulin sensitivity and increases energy expenditure in mice. Diabetes *58*, 1509–1517.

Guglielmi, G. (2018). How gut microbes are joining the fight against cancer. Nature *557*, 482–484.

Guilherme, A., Virbasius, J.V., Puri, V., and Czech, M.P. (2008). Adipocyte dysfunctions linking obesity to insulin resistance and type 2 diabetes. Nat. Rev. Mol. Cell Biol. *9*, 367–377.

Han, J., Gagnon, S., Eckle, T., and Borchers, C.H. (2013). Metabolomic analysis of key central carbon metabolism carboxylic acids as their 3-nitrophenylhydrazones by UPLC/ESI-MS. Electrophoresis *34*, 2891–2900.

Hangas, A., Aasumets, K., Kekäläinen, N.J., Paloheinä, M., Pohjoismäki, J.L., Gerhold, J.M., and Goffart, S. (2018). Ciprofloxacin impairs mitochondrial DNA replication initiation through inhibition of Topoisomerase 2. Nucleic Acids Res. *46*, 9625–9636.

Hill, D.A., Siracusa, M.C., Abt, M.C., Kim, B.S., Kobuley, D., Kubo, M., Kambayashi, T., Larosa, D.F., Renner, E.D., Orange, J.S., et al. (2012). Commensal bacteria-derived signals regulate basophil hematopoiesis and allergic inflammation. Nat. Med. *18*, 538–546.

Hoffmann, L.S., Etzrodt, J., Willkomm, L., Sanyal, A., Scheja, L., Fischer, A.W., Stasch, J.P., Bloch, W., Friebe, A., Heeren, J., and Pfeifer, A. (2015). Stimulation of soluble guanylyl cyclase protects against obesity by recruiting brown adipose tissue. Nat. Commun. *6*, 7235.

Hsiao, E.Y., McBride, S.W., Hsien, S., Sharon, G., Hyde, E.R., McCue, T., Codelli, J.A., Chow, J., Reisman, S.E., Petrosino, J.F., et al. (2013). Microbiota modulate behavioral and physiological abnormalities associated with neurodevelopmental disorders. Cell *155*, 1451–1463.

Iida, N., Dzutsev, A., Stewart, C.A., Smith, L., Bouladoux, N., Weingarten, R.A., Molina, D.A., Salcedo, R., Back, T., Cramer, S., et al. (2013). Commensal bacteria control cancer response to therapy by modulating the tumor microenvironment. Science *342*, 967–970.

Ikeda, K., Kang, Q., Yoneshiro, T., Camporez, J.P., Maki, H., Homma, M., Shinoda, K., Chen, Y., Lu, X., Maretich, P., et al. (2017). UCP1-independent signaling involving SERCA2b-mediated calcium cycling regulates beige fat thermogenesis and systemic glucose homeostasis. Nat. Med. *23*, 1454–1465.

Jiang, S., Li, T., Zhou, X., Qin, W., Wang, Z., and Liao, Y. (2018). Antibiotic drug piperacillin induces neuron cell death through mitochondrial dysfunction and oxidative damage. Can. J. Physiol. Pharmacol. *96*, 562–568.

Kaiko, G.E., Ryu, S.H., Koues, O.I., Collins, P.L., Solnica-Krezel, L., Pearce, E.J., Pearce, E.L., Oltz, E.M., and Stappenbeck, T.S. (2016). The Colonic Crypt Protects Stem Cells from Microbiota-Derived Metabolites. Cell *165*, 1708–1720.

Kalghatgi, S., Spina, C.S., Costello, J.C., Liesa, M., Morones-Ramirez, J.R., Slomovic, S., Molina, A., Shirihai, O.S., and Collins, J.J. (2013). Bactericidal antibiotics induce mitochondrial dysfunction and oxidative damage in Mammalian cells. Sci. Transl. Med. *5*, 192ra85.

Kau, A.L., Ahern, P.P., Griffin, N.W., Goodman, A.L., and Gordon, J.I. (2011). Human nutrition, the gut microbiome and the immune system. Nature *474*, 327–336.

Kazak, L., Chouchani, E.T., Jedrychowski, M.P., Erickson, B.K., Shinoda, K., Cohen, P., Vetrivelan, R., Lu, G.Z., Laznik-Bogoslavski, D., Hasenfuss, S.C., et al. (2015). A creatine-driven substrate cycle enhances energy expenditure and thermogenesis in beige fat. Cell *163*, 643–655.

Keipert, S., Kutschke, M., Ost, M., Schwarzmayr, T., van Schothorst, E.M., Lamp, D., Brachthauser, L., Hamp, I., Mazibuko, S.E., Hartwig, S., et al. (2017). Long-Term Cold Adaptation Does Not Require FGF21 or UCP1. Cell Metab. *26*, 437–446.e5.

Kind, T., Wohlgemuth, G., Lee, D.Y., Lu, Y., Palazoglu, M., Shahbaz, S., and Fiehn, O. (2009). FiehnLib: mass spectral and retention index libraries for metabolomics based on quadrupole and time-of-flight gas chromatography/mass spectrometry. Anal. Chem. *81*, 10038–10048.

Koeth, R.A., Wang, Z., Levison, B.S., Buffa, J.A., Org, E., Sheehy, B.T., Britt, E.B., Fu, X., Wu, Y., Li, L., et al. (2013). Intestinal microbiota metabolism of L-carnitine, a nutrient in red meat, promotes atherosclerosis. Nat. Med. *19*, 576–585.

Koh, A., Molinaro, A., Stahlman, M., Khan, M.T., Schmidt, C., Manneras-Holm, L., Wu, H., Carreras, A., Jeong, H., Olofsson, L.E., et al. (2018). Microbially Produced Imidazole Propionate Impairs Insulin Signaling through mTORC1. Cell *175*, 947–961.e17.

Ley, R.E., Bäckhed, F., Turnbaugh, P., Lozupone, C.A., Knight, R.D., and Gordon, J.I. (2005). Obesity alters gut microbial ecology. Proc. Natl. Acad. Sci. USA *102*, 11070–11075.

Li, F., Wu, R., Cui, X., Zha, L., Yu, L., Shi, H., and Xue, B. (2016). Histone Deacetylase 1 (HDAC1) Negatively Regulates Thermogenic Program in Brown

Adipocytes via Coordinated Regulation of Histone H3 Lysine 27 (H3K27) Deacetylation and Methylation. J. Biol. Chem. *291*, 4523–4536.

Li, L., Li, B., Li, M., Niu, C., Wang, G., Li, T., Król, E., Jin, W., and Speakman, J.R. (2017). Brown adipocytes can display a mammary basal myoepithelial cell phenotype in vivo. Mol. Metab. *6*, 1198–1211.

Li, Z., Yi, C.X., Katiraei, S., Kooijman, S., Zhou, E., Chung, C.K., Gao, Y., van den Heuvel, J.K., Meijer, O.C., Berbée, J.F.P., et al. (2018). Butyrate reduces appetite and activates brown adipose tissue via the gut-brain neural circuit. Gut *67*, 1269–1279.

Lopez, C.A., Kingsbury, D.D., Velazquez, E.M., and Bäumler, A.J. (2014). Collateral damage: microbiota-derived metabolites and immune function in the antibiotic era. Cell Host Microbe *16*, 156–163.

Lundberg, R., Toft, M.F., August, B., Hansen, A.K., and Hansen, C.H. (2016). Antibiotic-treated versus germ-free rodents for microbiota transplantation studies. Gut Microbes *7*, 68–74.

Maier, E., Anderson, R.C., and Roy, N.C. (2014). Understanding how commensal obligate anaerobic bacteria regulate immune functions in the large intestine. Nutrients *7*, 45–73.

Mariño, E., Richards, J.L., McLeod, K.H., Stanley, D., Yap, Y.A., Knight, J., McKenzie, C., Kranich, J., Oliveira, A.C., Rossello, F.J., et al. (2017). Gut microbial metabolites limit the frequency of autoimmune T cells and protect against type 1 diabetes. Nat. Immunol. *18*, 552–562.

Mayer, E.A., Tillisch, K., and Gupta, A. (2015). Gut/brain axis and the microbiota. J. Clin. Invest. *125*, 926–938.

Mills, E.L., Pierce, K.A., Jedrychowski, M.P., Garrity, R., Winther, S., Vidoni, S., Yoneshiro, T., Spinelli, J.B., Lu, G.Z., Kazak, L., et al. (2018). Accumulation of succinate controls activation of adipose tissue thermogenesis. Nature *560*, 102–106.

Moullan, N., Mouchiroud, L., Wang, X., Ryu, D., Williams, E.G., Mottis, A., Jovaisaite, V., Frochaux, M.V., Quiros, P.M., Deplancke, B., et al. (2015). Tetracyclines Disturb Mitochondrial Function across Eukaryotic Models: A Call for Caution in Biomedical Research. Cell Rep., S2211–1247(15)00180-1.

Nedergaard, J., Bengtsson, T., and Cannon, B. (2007). Unexpected evidence for active brown adipose tissue in adult humans. Am. J. Physiol. Endocrinol. Metab. *293*, E444–E452.

Nguyen, K.D., Qiu, Y., Cui, X., Goh, Y.P., Mwangi, J., David, T., Mukundan, L., Brombacher, F., Locksley, R.M., and Chawla, A. (2011). Alternatively activated macrophages produce catecholamines to sustain adaptive thermogenesis. Nature *480*, 104–108.

Nie, Y., Speakman, J.R., Wu, Q., Zhang, C., Hu, Y., Xia, M., Yan, L., Hambly, C., Wang, L., Wei, W., et al. (2015). ANIMAL PHYSIOLOGY. Exceptionally low daily energy expenditure in the bamboo-eating giant panda. Science *349*, 171–174.

Offermanns, S. (2017). Hydroxy-Carboxylic Acid Receptor Actions in Metabolism. Trends Endocrinol. Metab. *28*, 227–236.

Olsen, J.M., Csikasz, R.I., Dehvari, N., Lu, L., Sandström, A., Öberg, A.I., Nedergaard, J., Stone-Elander, S., and Bengtsson, T. (2017). β_3-Adrenergically induced glucose uptake in brown adipose tissue is independent of UCP1 presence or activity: mediation through the mTOR pathway. Mol. Metab. *6*, 611–619.

Olszak, T., An, D., Zeissig, S., Vera, M.P., Richter, J., Franke, A., Glickman, J.N., Siebert, R., Baron, R.M., Kasper, D.L., and Blumberg, R.S. (2012). Microbial exposure during early life has persistent effects on natural killer T cell function. Science *336*, 489–493.

Pfannenberg, C., Werner, M.K., Ripkens, S., Stef, I., Deckert, A., Schmadl, M., Reimold, M., Häring, H.U., Claussen, C.D., and Stefan, N. (2010). Impact of age on the relationships of brown adipose tissue with sex and adiposity in humans. Diabetes *59*, 1789–1793.

Qin, J., Li, R., Raes, J., Arumugam, M., Burgdorf, K.S., Manichanh, C., Nielsen, T., Pons, N., Levenez, F., Yamada, T., et al.; MetaHIT Consortium (2010). A human gut microbial gene catalogue established by metagenomic sequencing. Nature *464*, 59–65.

Rothwell, N.J., and Stock, M.J. (1979). A role for brown adipose tissue in diet-induced thermogenesis. Nature *281*, 31–35.

Saito, M., Okamatsu-Ogura, Y., Matsushita, M., Watanabe, K., Yoneshiro, T., Nio-Kobayashi, J., Iwanaga, T., Miyagawa, M., Kameya, T., Nakada, K., et al. (2009). High incidence of metabolically active brown adipose tissue in healthy adult humans: effects of cold exposure and adiposity. Diabetes *58*, 1526–1531.

Sealy, L., and Chalkley, R. (1978). The effect of sodium butyrate on histone modification. Cell *14*, 115–121.

Seedorf, H., Griffin, N.W., Ridaura, V.K., Reyes, A., Cheng, J., Rey, F.E., Smith, M.I., Simon, G.M., Scheffrahn, R.H., Woebken, D., et al. (2014). Bacteria from diverse habitats colonize and compete in the mouse gut. Cell *159*, 253–266.

Sivan, A., Corrales, L., Hubert, N., Williams, J.B., Aquino-Michaels, K., Earley, Z.M., Benyamin, F.W., Lei, Y.M., Jabri, B., Alegre, M.L., et al. (2015). Commensal Bifidobacterium promotes antitumor immunity and facilitates anti-PD-L1 efficacy. Science *350*, 1084–1089.

Sobrino, F., Gualberto, A., and Pintado, E. (1988). Regulation of fructose 2,6-bisphosphate levels in cold-acclimated brown adipose tissue of rat. FEBS Lett. *229*, 91–94.

Sommer, F., and Bäckhed, F. (2013). The gut microbiota–masters of host development and physiology. Nat. Rev. Microbiol. *11*, 227–238.

Speakman, J. (1997). Doubly Labelled Water: Theory and Practice (Springer).

Speakman, J.R. (2013). Evolutionary perspectives on the obesity epidemic: adaptive, maladaptive, and neutral viewpoints. Annu. Rev. Nutr. *33*, 289–317.

Suárez-Zamorano, N., Fabbiano, S., Chevalier, C., Stojanović, O., Colin, D.J., Stevanović, A., Veyrat-Durebex, C., Tarallo, V., Rigo, D., Germain, S., et al. (2015). Microbiota depletion promotes browning of white adipose tissue and reduces obesity. Nat. Med. *21*, 1497–1501.

Thackray, L.B., Handley, S.A., Gorman, M.J., Poddar, S., Bagadia, P., Briseno, C.G., Theisen, D.J., Tan, Q., Hykes, B.L., Jr., Lin, H., et al. (2018). Oral Antibiotic Treatment of Mice Exacerbates the Disease Severity of Multiple Flavivirus Infections. Cell Rep. *22*, 3440–3453.e6.

Tremaroli, V., and Bäckhed, F. (2012). Functional interactions between the gut microbiota and host metabolism. Nature *489*, 242–249.

Turnbaugh, P.J., Ley, R.E., Mahowald, M.A., Magrini, V., Mardis, E.R., and Gordon, J.I. (2006). An obesity-associated gut microbiome with increased capacity for energy harvest. Nature *444*, 1027–1031.

Turnbaugh, P.J., Bäckhed, F., Fulton, L., and Gordon, J.I. (2008). Diet-induced obesity is linked to marked but reversible alterations in the mouse distal gut microbiome. Cell Host Microbe *3*, 213–223.

Underhill, D.M., and Iliev, I.D. (2014). The mycobiota: interactions between commensal fungi and the host immune system. Nat. Rev. Immunol. *14*, 405–416.

Ussar, S., Griffin, N.W., Bezy, O., Fujisaka, S., Vienberg, S., Softic, S., Deng, L., Bry, L., Gordon, J.I., and Kahn, C.R. (2015). Interactions between Gut Microbiota, Host Genetics and Diet Modulate the Predisposition to Obesity and Metabolic Syndrome. Cell Metab. *22*, 516–530.

Vétizou, M., Pitt, J.M., Daillère, R., Lepage, P., Waldschmitt, N., Flament, C., Rusakiewicz, S., Routy, B., Roberti, M.P., Duong, C.P., et al. (2015). Anticancer immunotherapy by CTLA-4 blockade relies on the gut microbiota. Science *350*, 1079–1084.

Vijay, N., and Morris, M.E. (2014). Role of monocarboxylate transporters in drug delivery to the brain. Curr. Pharm. Des. *20*, 1487–1498.

Walsh, M.E., Bhattacharya, A., Sataranatarajan, K., Qaisar, R., Sloane, L., Rahman, M.M., Kinter, M., and Van Remmen, H. (2015). The histone deacetylase inhibitor butyrate improves metabolism and reduces muscle atrophy during aging. Aging Cell *14*, 957–970.

Wang, H., Liu, L., Lin, J.Z., Aprahamian, T.R., and Farmer, S.R. (2016). Browning of White Adipose Tissue with Roscovitine Induces a Distinct Population of UCP1$^+$ Adipocytes. Cell Metab. *24*, 835–847.

Yang, J.H., Bhargava, P., McCloskey, D., Mao, N., Palsson, B.O., and Collins, J.J. (2017). Antibiotic-Induced Changes to the Host Metabolic Environment

Inhibit Drug Efficacy and Alter Immune Function. Cell Host Microbe *22*, 757–765.e3.

Yano, J.M., Yu, K., Donaldson, G.P., Shastri, G.G., Ann, P., Ma, L., Nagler, C.R., Ismagilov, R.F., Mazmanian, S.K., and Hsiao, E.Y. (2015). Indigenous bacteria from the gut microbiota regulate host serotonin biosynthesis. Cell *161*, 264–276.

Zarrinpar, A., Chaix, A., Xu, Z.Z., Chang, M.W., Marotz, C.A., Saghatelian, A., Knight, R., and Panda, S. (2018). Antibiotic-induced microbiome depletion alters metabolic homeostasis by affecting gut signaling and colonic metabolism. Nat. Commun. *9*, 2872.

Zhao, L. (2013). The gut microbiota and obesity: from correlation to causality. Nat. Rev. Microbiol. *11*, 639–647.

Ziętak, M., Kovatcheva-Datchary, P., Markiewicz, L.H., Ståhlman, M., Kozak, L.P., and Bäckhed, F. (2016). Altered Microbiota Contributes to Reduced Diet-Induced Obesity upon Cold Exposure. Cell Metab. *23*, 1216–1223.

STAR★METHODS

KEY RESOURCES TABLE

REAGENT or RESOURCE	SOURCE	IDENTIFIER
Antibodies		
UCP1	Abcam	Cat# ab10983; RRID:AB_2241462
Total HSL	CST	Cat# 4107; RRID:AB_2296900
Phospho-HSL	CST	Cat# 4126; RRID:AB_490997
β-actin	ZSGB-Bio	Cat# TA-09; RRID:AB_2636897
PE-cy7 conjugated anti-CD45	eBioscience	Clone 30-F11; Cat# 25-0451; RRID:AB_469625
Percp-5.5 conjugated anti-CD11b	eBioscience	Clone M1/70; Cat# 45-0112-82; RRID:AB_953558
FITC conjugated anti-F4/80	BioLegend	Clone BM8; Cat# 123108; RRID:AB_893502
eF450 conjugated anti-CD11c	eBioscience	Clone N418; Cat# 48-0114-82; RRID:AB_1548654
PE conjugated anti-CD206	BioLegend	Clone C068C2; Cat# 141706; RRID:AB_10895754
AF647 conjugated anti-SiglecF	BD PharMingen	Clone E50-2440; Cat# 562680; RRID:AB_2687570
Fcγ blocker anti-CD16/CD32	eBioscience	Clone 93; Cat# 14-0161-85; RRID:AB_467134
Chemicals, Peptides, and Recombinant Proteins		
ampicillin	J&K	A01-290395
neomycin	J&K	A01-557926
gentamicin	J&K	A01-405947
metronidazole	J&K	J07-M0924
vancomycin	INALCO	1758-9326
sucralose	J&K	A01-442522
neomycin	Sigma	N6386
streptomycin	Sigma	S1277
penicillin	Sigma	P3032
vancomycin	Sigma	V2002
metronidazole	Sigma	M1547
bacitracin	Sigma	11702
ciprofloxacin	Sigma	17850
ceftazidime	Sigma	C3809
gentamycin	Sigma	G1914
[U^{13}C] butyrate	Sigma	488380
^{12}C butyrate	Sigma	303410
CL-316243	Sigma	C5976
IL-4	Peprotech	214-14
Trizol	Invitrogen	15596018
SYBR Green PCR kit	TransGen Biotech	EP1602
T-PER	ThermoFisher	78510
Protease inhibitor cocktail	Sigma	P8340
PMSF	Sigma	P7626
bicinchoninic acid (BCA) protein quantification kit	ThermoFisher	23227
Immobilon-P PVDF membranes	Millipore	ISEQ00010
ECL blotting reagents	GE Healthcare	RPN2232
mouse IL-4 ELISA kit	BioLegend	431107
mouse IL-5 Platinum kit	eBioscience	BMS610
mouse IL-33 Platinum kit	eBioscience	BMS6025
2-CAT (A-N) ELISA	LDN	BA-E5400

(*Continued on next page*)

Continued

REAGENT or RESOURCE	SOURCE	IDENTIFIER
Leptin ELISA kit	Crystalchem	90030
Insulin ELISA kit	Crystalchem	90080
circulating NEFA	Biovision	K612
Fecal genomic extraction kit	Tiangen	DP-328
Collagenase I	Sigma	C0130
Red blood cell lysis buffer	Tiangen	RT122-01
Experimental Models: Organisms/Strains		
Mouse: C57BL/6J-SPF	Vital River	N/A
Mouse: C57BL/6J-GF	SLAC laboratory animal, Shanghai	N/A
Oligonucleotide section		
Primers	Table S5	N/A
Deposited Data		
RNA-seq data	NCBI GEO	GSE117843
16S rDNA data	NCBI SRA	PRJNA514397
Software and Algorithms		
GraphPad version 6	N/A	N/A
Minitab 16	N/A	N/A
STAR v2.5.3	N/A	N/A
HTseq v0.6.1	N/A	N/A
R v3.4	N/A	N/A
DEseq2 v1.20.0	N/A	N/A
QIIME2	N/A	N/A

CONTACT FOR REAGENT AND RESOURCE SHARING

Further information and requests for resources and reagents should be directed to the Lead Contact, John R. Speakman (j.speakman@abdn.ac.uk).

EXPERIMENTAL MODEL AND SUBJECT DETAILS

7-8 week old male wild-type (Control) C57BL/6J mice were purchased from Vital River, Beijing. 11-12 week old male Germ free mice (GF) and respective C57BL/6J Controls (SPF) were acquired from SLAC laboratory animal, Shanghai. All animal procedures were approved by the Institute of Genetics and Developmental Biology Chinese Academy of Sciences (IGDB-CAS) Institutional Review Board Approval numbers for the various experiments are AP2016026, AP2016029, AP2016030, AP2016031 and AP2016032. Mice were maintained under SPF facility in 12h:12h day and night cycles at 23 ± 1°C and fed standard chow diet (20% Protein, 70% Carbohydrate and 10% Fat, #D12450B, Research Diets, New Brunswick, NJ, USA). Mice were provided with autoclaved drinking water. Antibiotics were administered in the sterile drinking water *ad libitum* and changed every 3 days, ABX protocol containing ampicillin (0.5 mg/mL, J&K), neomycin (0.5 mg/mL, J&K), gentamicin (0.5 mg/mL, J&K), metronidazole (0.5 mg/mL, J&K), vancomycin (0.25 mg/mL, INALCO), and sucralose (4 mg/mL, Splenda, J&K) (Abt et al., 2012). ABX-SZ protocol containing neomycin (100 μg/mL, Sigma), streptomycin (50 μg/mL, Sigma), penicillin (100 U/mL, Sigma), vancomycin (50 μg/mL, Sigma), metronidazole (100 μg/mL, Sigma), bacitracin (1 mg/mL, Sigma), ciprofloxacin (125 μg/mL, Sigma), ceftazidime (100 μg/mL, Sigma) and gentamycin (170 μg/mL, Sigma) (Suárez-Zamorano et al., 2015). [$U^{13}C$] butyrate (488380, Sigma) and ^{12}C butyrate (303410, Sigma) were dissolved in PBS (160 mg/mL). Antibiotic treatment started in 8-9 weeks old animals for 3-4 weeks. For the thermoneutrality experiments, mice were adapted to 30°C in a laboratory incubator (Jiangnan Instruments) for 3 weeks before manipulation. For the cold challenge experiments, mice were fed *ad libitum* and individually housed in cages at 4°C. Tissues, feces contents and serum were collected at the end of each experiment and quickly snapped in liquid nitrogen then stored in −80°C for further experiments. For pair feed (PF) experiment, we measured the assimilation efficiency of Control mice and ABX mice every day. We assumed that the digestive efficiency of PF mice is similar as Control mice, and PF mice were given quota food following the linear relationship between ABX food intake and ABX body weight.

METHOD DETAILS

Metabolic phenotype analysis

We used magnetic-resonance whole-body composition analyzer (EchoMRI, Houston, TX) to analyze mice body composition (fat mass, lean mass and water content). We measured food intake and collected the feces every 24h. The feces were dried at 60°C for 7 days then subjected to an oxygen bomb calorimeter (Parr, 1281, USA) to measure the calorie excretion of feces. We assessed energy expenditure and physical activity by using indirect calorimetric system (TSE PhenoMaster, TSE Systems, Bad Homburg, Germany). Daily energy expenditure (DEE) of GF and SPF mice were measured by the DLW ($^2H_2{}^{18}O$) technique (Nie et al., 2015). To assess the effect of β3-adrenergic agonist CL-316243 on the energy expenditure, we treated mice daily for 3 consecutive days through intraperitoneal administration of either vehicle (PBS) or CL-316243 (1 mg/kg). To assess the effect of IL-4 (50 μg/kg) on energy expenditure, we treated mice daily for 5 consecutive days through intraperitoneal administration of either vehicle (PBS) or IL-4. During the whole experimental manipulation, mice were housed in the metabolic chambers of TSE machine.

Quantitative PCR

Tissues were homogenized in Trizol (Invitrogen) by Bead Ruptor (OMNI). Total RNA was isolated using chloroform/isopropyl alcohol and 3 μg total RNA was used as the template for cDNA synthesis (Invitrogen). Real-time PCR was performed using SYBR Green PCR kit (TransGen Biotech) and quantitative PCR reaction was carried out in triplicate using 384 well PCR microplate for LightCycler 480 II (Roche). The relative expression levels of each gene were normalized to housekeeping gene TATA-box binding protein (*Tbp*), the specificity of amplified genes was verified by dissociation curves. RNA expression data were analyzed according to the $-\Delta\Delta C_t$ method.

Western blotting

The whole adipose tissue pads were homogenized in tissue protein extraction reagent supplemented with a protease inhibitor cocktail and 10 mM PMSF and the lysates were chilled on ice for 30 min then centrifuged at 12,000 rpm (10 min) to remove cell debris. The supernatant was collected then the protein concentration was measured by bicinchoninic acid (BCA) protein quantification kit. Equal amounts of protein were separated on 12% SDS-PAGE gels and blotted onto Immobilon-P PVDF membranes. After blocking in 5% skim milk in PBS-T (PBS with 0.05% Tween-20) for 1 hour at room temperature, membranes were incubated with primary antibody at 4°C overnight. To visualize the bands, HRP-labeled secondary antibodies and ECL blotting reagents (GE Healthcare) were used. The bands were quantified with ImageJ 1.50i software. The primary antibodies used for western blot were UCP1 (#ab10983, diluted 1:3,000, Abcam), Total HSL (#4107, diluted 1:2,000, CST), Phospho-HSL (Ser660) (#4126, diluted 1: 2,000, CST), β-actin (#AB1015T, diluted 1:5,000, AmeriBiophama).

Histology

10 μm paraffin slice of SPF and GF groups were incubated with xylene for 1min then step rehydration from gradient alcohol to PBS. The slices were incubated with the hematoxylin for 2 min then stained eosin for 2min. The dehydrated slices were sealed by neutral balsam.

Hormone measurements

The subcutaneous WAT (scWAT) was homogenized in tissue protein extraction reagent. Total protein was extracted and the concentration was measured using BCA protein quantification kit. The content of cytokines and norepinephrine in local scWAT were determined by ELISA kits. IL-4 was measured by mouse IL-4 ELISA kit (#431107, BioLegend). IL-5 and IL-33 were measured by Platinum ELISA (#BMS610, #BMS6025, eBioscience). Norepinephrine was measured by 2-CAT (A-N) Research ELISA (#BA-E5400, LDN). Circulating Leptin and Insulin were measured by Crystalchem INC and circulating NEFA was measured by FFA Quantification Colorimetric/Fluorometric Kit (#K612, Biovision). Triglycerides (GPO-PAP method), total cholesterol (CHOD-PAP method), high density lipoprotein cholesterol (direct method) and low-density lipoprotein cholesterol (direct method) in circulating were analyzed on the auto clinical chemistry analyzer platform (ZY-330, KHB). Blank Control and quality Controls were added in every measurement. All the processes were administrated according to the manufacturer's instructions.

^{13}C enrichment in breath samples

The technique we have developed for the measurement of butyrate homeostasis using [$U^{13}C$] butyrate involves oral gavage. The mice were fasted 8 hours before the experiment and transferred to a small chamber with a constant gas flow after the gavage treatment. The flow is regulated such that the outflow CO_2 is around 0.5%. This is 20x higher than the atmospheric CO_2 hence incoming CO_2 has only a negligible impact on the measurements. The outflow stream is then sampled at 10-minute intervals by collecting gas into a standard vacutainer for up to 200 minutes. The air samples were analyzed using an auto-sampler linked to a conventional gas source isotope ratio mass spectrometer (Microgas uG). [$U^{13}C$] butyrate in circulation entered cells and then is metabolized appearing as $^{13}CO_2$ in the breath. Hence by collecting breath and measuring the ^{13}C:^{12}C ratio in respiratory CO_2 this provides an indication of the rate of butyrate clearance from the body. This provides real time read out of the butyrate in a stress free and more detailed manner than the standard test provides.

Quantitative analysis of SCFA and TCA cycle metabolites

Mice were orally administrated [U^{13}C] and ^{12}C butyrate sodium (80mg, 1:10 ratio) and harvested tissue after 1-hour treatment. Samples were immediately frozen by dry ice before LC–MS analysis. SCFA and TCA cycle metabolite measurement and isotope tracing were conducted via HPLC-MS/MS at LipidALL Technologies. In brief, SCFAs and TCA cycle metabolites were extracted from various biological materials (serum, feces, cecum, colon and adipose) using solvent mixtures containing acetonitrile and water. The extract was then derivatized with 3-nitrophenylhdyrazones and analyzed on a ThermoFisher DGLC-3000 coupled to Sciex QTRAP 6500 Plus system. Individual metabolites were separated on a Phenomenex Kinetex C18 column (100 × 2.1 mm, 2.6 μm) using 0.1% formic acid in water as mobile phase A and 0.1% formic acid in acetonitrile as mobile phase B. The gradient started with 15% B which increases linearly to 100% over 12 min, followed by a re-equlibration at 15% B over 3 min before the next injection. Octanoic acid-1-$^{13}C_1$ purchased from Sigma-Aldrich was used as an internal standard for quantitation, and molar responses of individual SCFAs were corrected against that of octanoic acid for accurate quantitation Details of the analysis had been previously published elsewhere (Han et al., 2013).

Serum metabolites

Serum metabolites were measured and analyzed by GC-TOF-MS at the Biotree corporation. We dried the serum extracts in a vacuum concentrator without heating. Add 30 μL methoxyamination hydrochloride (20 mg/mL in pyridine), incubation for 30min at 80°C. Add 40 μL of the BSTFA regent (1% TMCS, v/v) to the sample aliquots, incubated for 2h at 70°C. Add 10 μL FAMEs (Standard mixture of fatty acid methyl esters, C8-C16: 1mg/mL; C18-C24: 0.5mg/mL in chloroform) to the QC sample it cooling to the room temperature. GC-TOF-MS analysis was performed using an Agilent 7890 gas chromatograph system coupled with a Pegasus HT time-of-flight mass spectrometer. The system utilized a DB-5MS capillary column coated with 5% diphenyl cross-linked with 95% dimethylpolysiloxane (30 m × 250 μm inner diameter, 0.25 μm film thickness; J&W Scientific, Folsom, CA, USA). A 1 μL aliquot of the analyte was injected in splitless mode. Helium was used as the carrier gas, the front inlet purge flow was 3mL min^{-1}, and the gas flow rate through the column was 1mL min^{-1}. The initial temperature was kept at 50°C for 1 min, then raised to 300°C at a rate of 20°C min^{-1}, then kept for 6.5min at 300°C.The injection, transfer line, and ion source temperatures were 280, 270, and 220°C, respectively. The energy was −70eV in electron impact mode. The mass spectrometry data were acquired in full-scan mode with the m/z range of 50–500 at a rate of 20 spectra per second after a solvent delay of 371 s. Chroma TOF 4.3X software of LECO Corporation and LECO-Fiehn Rtx5 database were used for raw peaks exacting, the data baselines filtering and calibration of the baseline, peak alignment, deconvolution analysis, peak identification and integration of the peak area (Kind et al., 2009). The RI (retention time index) method was used in the peak identification, and the RI tolerance was 5000.

RNA-seq and Bioinformatics

Total RNA from fat tissue were extracted by the RNeasy Mini Kit (QIAGEN) according to manufacturer's recommendations and validated by the Agilent 2100 Bioanalyzer. Sequencing libraries were generated using NEBNext® Ultra DNA Library Prep Kit for Illumina® (NEB, USA) and 150 bp paired-end reads were sequenced on Illumina Hiseq Xten platform in CapitalBio technology corporation (Beijng). Full sequencing data are available online at NCBI GEO (GSE117843). The paired-end clean reads were aligned to the reference genome (mm10) using STAR and each gene reads numbers were count by HTseq. Differential expression gene (DEG) analysis was performed by DEseq2 package in which gene length and dispersion bias was corrected. The resulting P values were adjusted using the Benjamini and Hochberg's approach for controlling the false discovery rate (FDR). Genes with an adjusted P value < 0.05 found by DESeq2 were assigned as differentially expressed.

16S rDNA qPCR and Amplicon Sequencing

Fecal pellets were immediately frozen in liquid nitrogen after collection and stored at −80°C. Fecal nucleic acid was extracted from fecal pellets using Fecal genomic extraction kit (DP-328, Tiangen technology corporation). SYBR green quantitative PCR for bacterial 16S rRNA genes was performed using primers 515F and 806R. Quantitation of 16S rRNA genes was performed by comparison to a plasmid standard control of pUC57 containing a 16S rRNA sequence from an uncultured intestinal bacterium from mice (Thackray et al., 2018). Barcoded PCR primers (341F and 805R) directed at the V3/V4 region of bacterial 16S rRNA genes were used to generate libraries and libraries were validated by the Agilent 2100 Bioanalyzer. Sequencing were performed with 250 bp paired-end reads on Illumina Hiseq2500 platform in Annoroad Gene Technology (Beijng). The paired-end clean reads were aligned to the reference genome (SILVA_132) using QIIME2.

Flow cytometry

Primary stromal vascular fractions (SVF) from BAT, scWAT and pgVAT were prepared to FACS analysis. Details of the analysis had been previously published elsewhere (Li et al., 2017). In brief, tissues were freshly collected, washed by pre-warm PBS at 37°C and dissociated by scissors and then incubated with DMEM medium containing 5% fetal bovine serum, 3 mg/mL collagenase I (Sigma) for 60 min at 37°C. The digested cell suspension was centrifuged at 500 g for 5 min to separate stromal-vascular fraction from adipocytes. The pelleted cells were incubated with 0.25% trypsin-EGTA for 3 min, then re-suspended in 5 mg/mL Dispase and 50 IU/mL DNaseI for 5 min, erythrocytes were removed by red blood cell lysis for 3 min before filtration through a 40-μm cell mesh to remove large cellular debris. After cell suspension, cells were incubated in FACS buffer (PBS with 5% FBS and 1%

Penicillin-Streptomycin) in the presence of staining antibody. The following primary antibodies were used: PE-cy7 conjugated anti-CD45 (eBioscience, Clone 30-F11), Percp-cy5.5 conjugated anti-CD11b (eBioscience, Clone M1/70), FITC conjugated anti-F4/80 (BioLegend, Clone BM8), eFluor450 conjugated anti-CD11c (eBioscience, Clone N418), PE conjugated anti-CD206 (BioLegend, Clone C068C2), Alexa Fluor 647 conjugated anti-SiglecF (BD PharMingen, Clone E50-2440), Fcγ blocker anti-CD16/CD32 (eBioscience, Clone 93). The positive antibody signals were gated based on fluorescence minus one (FMO) Control every time. Data was acquired on BD FACS Aria II and data analysis was performed using FlowJo v7.6.1 software.

Thermal conductance of pelage

The thermal conductance of pelage was measured as described in our previous study (Corp et al., 1997). In brief, the pelage was removed by making a longitudinal ventral incision from the throat to the anus and then separating the pelage from the body cavity. Pelages were stored at 4°C until assayed (1-3 days). We wrapped the pelage around a small bottle filled with water (20 mL) that contained a temperature transmitter (iButton, DS2422, USA), and then attached it to the bottle with contact adhesive. An incubator was used to heat the bottle of water to 40°C. After reaching 40°C, the bottle was immediately put into another incubator at 20°C, and then the temperature, decreasing from 40 to 20°C, was monitored every 10 s. Each data point was transformed according to ln(x-20), where x is the temperature monitored during the temperature decreasing course. The slope calculated for these transformed data was defined as thermal conductance.

QUANTIFICATION AND STATISTICAL ANALYSIS

Replicate information is indicated in the figure legends. All results are given as mean ± SEM and analyzed by using statistical tools implemented in Prism (GraphPad version 6). Statistical analyses were performed using the Student's t test and regular one-way or two-way analysis of variance (ANOVA). Differences with $p < 0.05$ were considered to be significant. $p < 0.05$ (*), $p < 0.01$ (**), $p < 0.001$ (***) and $p < 0.0001$ (****).

DATA AND SOFTWARE AVAILABILITY

The transcriptomics data for Figures 5 and S6 is now deposited at GEO (the accession number for the transcriptomics data is GEO: GSE117843). The 16S rDNA data for Figures 6 and S7 is now deposited at SRA (the accession number for the 16S rDNA data is SRA: PRJNA514397).